GEORGIA INSTITUTE OF TECHNOLOGY
OFFICE OF CONTRACT ADMINISTRATION
SPONSORED PROJECT INITIATION

Date: 12/30/80

Project Title: The Effect of Microstructure on the Properties of High Strength Al uminum Alloys

Project No: E-19-636 (continuation of E-19-603)

Project Director: Dr. E. A. Starke, Jr.

Sponsor: Air Force Office of Scientific Research; Bolling AFB, D. C. 20332

Agreement Period: From 1/1/81 Until 12/31/81 (04 year)

Type Agreement: Grant No. AFOSR-78-3471D

Amount: $140,000 AFOSR
40,860 GIT (E-19-353)
$180,860 TOTAL

Reports Required: Informal Technical Reports; Final Technical Report

Sponsor Contact Person (s):

Technical Matters

Dr. Alan H. Rosenstein
Program Manager
Directorate of Electronic &
Solid State Sciences
Building 410
Bolling AFB, D. C. 20332
(202) 767-4931

Contractual Matters
(thru OCA)

Ms. Joan O. Marshall
Contracting Officer
Department of the Air Force
Air Force Office of Scientific Research
Building 410
Bolling AFB, D. C. 20332
(202) 767-4877

Defense Priority Rating: None

Assigned to: Chemical Engineering (School/Laboratory)

COPIES TO:

Project Director
Division Chief (EES)
School/Laboratory Director
Dean/Director—EES
Accounting Office
~~Procurement Office~~
Security Coordinator (OCA)
~~Reports Coordinator (OCA)~~
Library, Technical Reports Section
EES Information Office
EES Reports & Procedures
Project File (OCA)
Project Code (GTRI)
Other OCA Research Property Coordinator

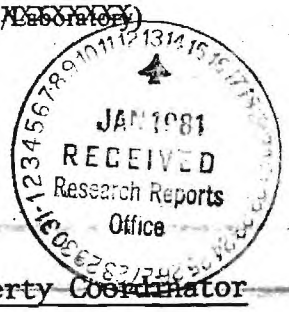

CA—3 (3/76)

GEORGIA INSTITUTE OF TECHNOLOGY OFFICE OF CONTRACT ADMINISTRATION

SPONSORED PROJECT TERMINATION SHEET

Date 6/30/83

Project Title: "The Effect of Microstructure on the Properties of High Strength Aluminum Alloys"

Project No: E-19-636

Project Director: Dr. E. A. Starke, Jr.

Sponsor: Air Force Office of Scientific Research/Bolling AFB

Effective Termination Date: 12/31/82

Clearance of Accounting Charges: 12/31/82

Grant/Contract Closeout Actions Remaining:

- ☐ **Final Invoice and Closing Documents**
- ☐ **Final Fiscal Report**
- ☐ Final Report of Inventions
- ☐ Govt. Property Inventory & Related Certificate
- ☐ Classified Material Certificate
- ☐ Other _____

None: (04 year)
Continued by E-19-615 (05 year) due to change in OH rates. The 03 year was E-19-603; it was terminated 12/80.

Assigned to: Chemical Engineering (School/~~Laboratory~~)

COPIES TO:

Administrative Coordinator	Research Security Services	EES Public Relations (2)
Research Property Management	Reports Coordinator (OCA) ✓	Computer Input
Accounting	Legal Services (OCA)	Project File
Procurement/EES Supply Services	Library	Other Proj. Dir.

Georgia Institute of Technology

ATLANTA, GEORGIA 30332

OFFICE OF CONTRACT ADMINISTRATION

Telex: 542507 GTRIOCAATL
Fax: (404) 894-3120
Phone: (404) 894 - 4814

24 August 1981

Refer To: JG/G404.81-21

Department of the Air Force
Air Force Office of Scientific Research
Building 410
Bolling Air Force Base, D.C. 20332

Attention: Dr. Alan H. Rosenstein
Electronic and Solid State Sciences

Subject: Research Proposal Entitled, "The Effect of Microstructure on the Properties of High Strength Aluminum Alloys" (Continuation of Grant No. AFOSR-78-3471)

Gentlemen:

The GEORGIA INSTITUTE OF TECHNOLOGY desires to submit for your consideration the subject proposal prepared by Dr. E. A. Starke, Jr., Professor, School of Chemical Engineering. This is for a continuation of the work currently being conducted under Grant No. AFOSR-78-3471.

We believe you will find the proposal complete; however, if anything additional is desired, please let us know. Any matters pertaining to the scientific program or personnel may be referred to Dr. Starke at 404/894-2880. Administrative or contractual matters may be referred to the writer at 404/894-4814.

We appreciate the opportunity of submitting this proposal and look forward to the possibility of working with you on this program.

Sincerely,

Terry Goldbaugh
Contracting Officer

JG/arj

Addressee: Six (6) copies
Enclosure: Proposal - six (6) copies

THE EFFECT OF MICROSTRUCTURE ON THE PROPERTIES OF HIGH STRENGTH ALUMINUM ALLOYS

RENEWAL RESEARCH PROPOSAL FOR

GRANT NO. AFOSR-78-3471

THE EFFECT OF MICROSTRUCTURE ON THE PROPERTIES OF HIGH STRENGTH ALUMINUM ALLOYS

SUBMITTED TO
AIR FORCE OFFICE OF SCIENTIFIC RESEARCH

BY THE
GEORGIA INSTITUTE OF TECHNOLOGY
ATLANTA, GEORGIA 30332

Dr. Edgar A. Starke, Jr.
Principal Investigator
Professor of Metallurgy
Director, Fracture and Fatigue
Research Laboratory
Phone: 404/894-2880

Dr. Gary W. Poehlein, Director
School of Chemical Engineering

W. M. Sangster
Dean, College of Engineering

Jerry Goldbaugh
Contracting Officer

TABLE OF CONTENTS

I. INTRODUCTION

High strength/density ratios have made age-hardenable aluminum alloys extremely attractive for use in aircraft structures. Despite this superior property, limited corrosion, fatigue, and fracture resistance has restricted their commercial usage in maximum strength tempers. The problem of stress corrosion and exfolliation corrosion resistance has been greatly alleviated by the introduction of the T73 and T76 tempers(1) and research on this Grant has shown the importance of microstructure and composition in improving current SCC properties (2). More acceptable fracture toughness values have been obtained in the recently developed alloys such as 7175, 7475 and 7050 (3), largely as a result of increased alloy purity and specialized processing controls. Based on increased levels of toughness and SCC resistance the new aluminum alloys have increased the reliability or "life" of structural aircraft components. However, further improvements in component performance will necessarily be based on higher levels of fatigue resistance, and elastic modulus and decrease in density.

The inhomogeneous microstructure of aluminum alloys is fundamental to the fatigue problem. Failure of metals by fatigue is characterized by local slip in soft areas of high stress concentration, leading eventually to the formation of a macroscopic crack. Fatigue failure is not accompanied by the extensive yielding that occurs with static failure and local inhomogeneities are much more detrimental. Consequently, alloy development for fatigue resistance is more difficult than for static strength and fracture toughness, since the elimination of local inhomogeneities appears necessary. One of the long-term objectives of the research on this AFOSR-sponsored program is to obtain improved fatigue resistance in aluminum alloys by characterizing the fatigue process and establishing a better understanding of fatigue mechanisms in aircraft materials in terms of the microstructural variations produced by both composition and processing.

Besides beryllium, which has associated manufacturing and health related problems, lithium is the only known metal which improves both the modulus and density when alloyed with aluminum. Each weight percent lithium added to an aluminum alloy reduces the density approximately 3% and increases the elastic modulus approximately 6% (4) for lithium additions up to 4%. The development of Al-base alloys containing lithium began in Germany in the 1920's and was primarily concerned with additions of small amounts of lithium to age hardening alloys in order to increase their strength. In the 1950's metallurgists at Alcoa recognized that lithium increased the elastic modulus of aluminum and

developed the high strength Al-Cu-Li alloy 2020. However, the alloy had low ductility and fracture toughness in the maximum strength temper, and these limitations, along with production problems led to its withdrawal as a commercial alloy in 1969. Our research has shown that the low ductility and fracture toughness of 2020 is associated with strain localization problems (5,6). The research on this AFOSR-sponsored program on Al-Li alloys is directed toward understanding the strain localization problem and preventing its occurrence.

An extensive review of the current state of the art with respect to fatigue-microstructure relationships and the microstructure and properties of high modulus Al-Li alloys has been given in our previous proposals and will not be repeated here. The research conducted at Georgia Tech under AFOSR sponsorship has shown that microstructure plays an important role in both fatigue crack initiation and propagation behavior (7-16). Some microstructural features which are advantageous and some that are detrimental to fatigue resistance have been identified and are described in the referenced publications. Our recent research on Al-Li-X alloys have identified microstructural features which adversely affect the environmental sensitivity and fracture resistance of these promising alloys (5,6,17-21). Some suggested modifications which may result in improved properties are described in the referenced publications and are being evaluated in our current research.

Scope of Program on the Fatigue of 7XXX Alloys

Recent studies by the Air Force have shown that 50% of all material failures in aircraft are a result of fatigue (22). This high incidence of failures prompted the new safe-crack-growth approach for the design of new aerospace structural systems. However, accurate calculations require a knowledge of fatigue crack growth behavior under a wide variety of load and environmental conditions. Consequently, understanding the mechanisms involved in the initiation and propagation of fatigue cracks in metals is one of the key factors in designing aircraft that are safe, effective, and economical. Our program is microstructurally oriented and relies on both cyclic-stress-strain response (LCF) and crack growth studies in inert and corrosive environments with the objectives of:

1. Relating the microstructural features which can be controlled by processing with the fatigue performance of high strength aluminum alloys.
2. Establishing the role of deformation mode on the environmental sensitivity of the fatigue behavior of 7XXX alloys.

3. Combining microstructure and mechanical concepts for evaluating and predicting crack growth behavior of aluminum alloys.

Scope of Program on Microstructure-Properties of Al-Li-X Alloys

A significant weight savings can be obtained in the new aerospace systems planned for the next decade if aluminum alloys exhibiting 15% or more increased modulus coupled with 11% or more decreased density with respect to 7075 can be developed. Al-Li-X alloys are very attractive for stiffness-critical airframe components, since they have an excellent combination of low density and high modulus. However, their use has been limited by low fracture toughness and poor corrosion resistance. The long term objective of this phase of our program is to solve these problems through microstructure manipulation so that the utilization of these attractive alloys can be realized.

The program has the objectives of:

1. Establishing the role of impurity elements on the fracture behavior of Al-Li alloys.
2. Establishing the role of third and fourth element additions to Al-Li alloys and their effect on both chemical and mechanical properties.
3. Establishing the role of deformation mode and PFZ on the fracture behavior of Al-Li-X alloys.

II. PROGRESS DURING THE CURRENT YEAR

A. ABSTRACT

This program was initiated on 1 January 1978. During this program year the effect of copper content (from 0.01 to 2.1%) on the LCF behavior of four Al-6Zn-2Mg-XCu-T7351 alloys was investigated in laboratory air and dry air and compared with a previous study of the T651 condition. This research was designed to study the effect of copper content independent of variations in degree of coherency of the precipitates. Incoherent strengthening precipitates were obtained for all alloys by using the overaging, T7351 treatment. Unlike the results of the T651 study, no difference in the strain-life behavior was observed for the four alloys in either environment. Cyclic softening was observed and associated with grain boundary and slip band crack initiation and subsequent microcrack coalescence. The departure from linearity observed in the strain-life plots for both the peak aged and overaged conditions is associated with the fatigue crack initiation mechanism. Cracks are initiated at grain boundaries at high strain amplitudes and at slip bands at low strain amplitudes. Both mechanisms are possible at intermediate amplitudes.

The microstructure and tensile properties of two Al-3wt%Li-2wt%Cu-0.2wt%Zr alloys, one Cd-free and one containing 0.2wt%Cd, have been investigated. The Cd-free alloy remained unrecrystallized for all solutionizing treatments studied; whereas a special treatment had to be developed to prevent recrystallization during solutionizing of the 0.2wt% Cd alloy. In combination with cadmium, zirconium enters into the T_2 phase during high temperature processing. This reduces the volume fraction of the Al_3Zr phase which normally inhibits recrystallization. Consequently, a low temperature anneal to precipitate Al_3Zr is necessary prior to high temperature solutionizing in order to prevent recrystallization in the Cd-containing alloy. Unlike its effect in lower lithium, higher copper content aluminum alloys, cadmium does not significantly affect the nucleation of the strengthening precipitates. If anything, cadmium has a detrimental effect on the age hardening response of this alloy since it increases the formation of coarse Al-Cu-Li equilibrium phases at grain and subgrain boundaries and thus removes some of the copper and lithium from participating in the formation of the strengthening precipitates T_1 and δ'. Subgrain boundary fracture occurred during tensile tests of both alloys in the unrecrystallized condition; however, transgranular fracture occurred in tests of the partially recrystallized 0.2wt% Cd alloy. Both types of fractures are believed due to a form of strain localization associated with precipitate free zones and shearable precipitates.

B. SUMMARY

1. LCF of Al-6Zn-2Mg-XCu Alloys in the T7351 Condition

1.1 Cyclic Stress-Strain Response

The cyclic hardening and softening behavior for the four alloys in the T7351 condition were similar regardless of copper content and test environment. Representative curves for the 1% Cu alloy tested in dry air are shown in Fig. 1. All samples cycled at high plastic strain amplitudes harden slightly in the first few cycles until saturation and then soften. For the very low plastic strain amplitude no hardening was observed for most cases, and some samples showed softening from the first cycle. It is important to note that the cyclic softening is clearly identified by a gradual decrease of both the tensile and compressive stress with increasing number of cycles.

Cyclic softening has been observed in a high purity ITMT 7475 alloy (23) and attributed to the removal of residual stresses produced during quenching from the solutionizing temperature (the samples were not stretched prior to aging). Other investigations have associated cyclic softening with precipitate resolution during cyclic loading, aging inhomogeneities (24,25), and a disordering mechanism (26). These mechanisms may not apply for this study. Since softening was observed for samples tested in both dry air and laboratory air environments, softening is regarded as a mechanical and not an environmental effect. The four alloys were overaged to produce partially coherent and/or incoherent precipitates which are not sheared by dislocations during deformation. Extensive TEM examination of foils from LCF samples of all alloys for both high and low strain amplitudes revealed a uniform deformation structure. Extensive strain localization, found in the lower Cu content alloys of the T651 condition (11), was not observed. Consequently, it is believed that other factors may be involved in the cyclic softening process.

LCF samples, cycled to about 30% of N_f (number of cycles for complete failure), were examined by optical microscopy. Numerous grain boundary cracks were found for the high plastic strain amplitudes (e.g., $\Delta\varepsilon_p/2 = 1.025\%$). Crack initiation at grain boundaries may be associated with grain boundary precipitates and PFZ's present in the overaged alloys. Both grain boundary and slip band cracks were present for the intermediate plastic strain amplitudes (e.g., $\Delta\varepsilon_p/2 = 0.188\%$) and slip band cracks for the low plastic strain amplitudes (e.g., $\Delta\varepsilon_p/2 = 0.055\%$). This evidence suggests that the cyclic softening observed in this study is associated with the initiation of microcracks and the subsequent

coalescence of these cracks. It should be noted that in all cases macroscopic crack propagation was transgranular and normal to the stress axis.

Values of the cyclic strain hardening exponent, n', were determined from plots of the maximum stress versus the plastic strain amplitude. The values for the different alloys were essentially the same and correlate well with the deformation mode.

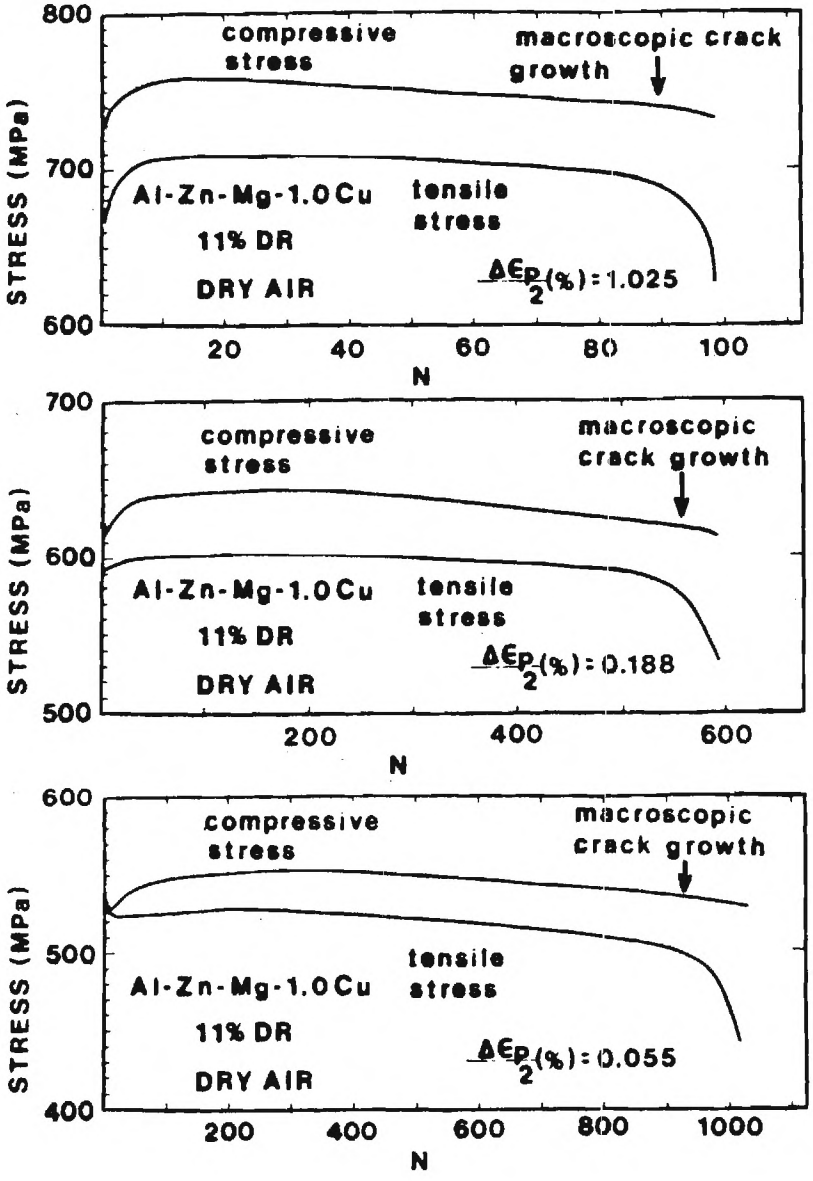

Figure 1. Cyclic hardening and softening curves for the 1.0% Cu alloy tested in dry air for various plastic strain amplitudes.

1.2 Strain-Life Behavior

Cyclic plastic strain creates fatigue damage and consequently, the fatigue life may be related to the plastic strain amplitude. The strain-life curves (Coffin-Manson plots) of Fig. 2 show that the low cycle fatigue life of the four alloys in the T7351 condition is not significantly affected by changes in humidity. These results are different from those obtained previously for the T651 condition for which an environmental effect, that increased with decreasing Cu content, was observed. Fractographic results substantiate the same trend with respect to the LCF resistance, i.e., the four alloys exhibited ductile striations regardless of the test environment. The environmental sensitivity was related to the deformation mode and the homogeneity of deformation; being greatest for the cases where extensive strain localization was observed. Our present results are consistent with this explanation. Since the strengthening precipitates of all the alloys are incoherent in the T7351 condition, they are looped and/or bypassed by dislocations. Consequently, the deformation is relatively homogeneous and environmental sensitivity is minimal.

Figure 3 shows a superposition of the strain-life curves for the four alloys in both dry and laboratory air. No effect of Cu content on the LCF life was observed. Again, this result is somewhat different from that obtained previously for the same alloys in the T651 condition (11). That study showed that the strain-controlled fatigue life increased with Cu content. In the T651 condition, the coherency of the strengthening precipitates decreases with increasing Cu content and this alters the deformation mode from dislocations shearing the precipitates (which leads to strain localization) to dislocations looping the precipitates (which leads to homogeneous deformation). This shift in deformation behavior delays fatigue crack initiation and increases the overall fatigue life. Since all alloys exhibited homogeneous deformation in the T7351 condition, the Cu content did not affect the fatigue life.

Figure 3 shows that a change of slope occurs in the Coffin-Manson plots of all alloys. Our recent unpublished work shows similar changes occurred at the same strain amplitude for the T651 condition. The data was replotted as plastic strain amplitude versus reversals to initiation instead of reversals to failure. The number of reversals to initiation was taken at the point where macroscopic crack propagation began, not when microcracks were first observed. This point could be detected by examination of the stress-cycles curves such as those shown in Fig. 1. Macroscopic crack growth (transgranular and normal to the stress axis)

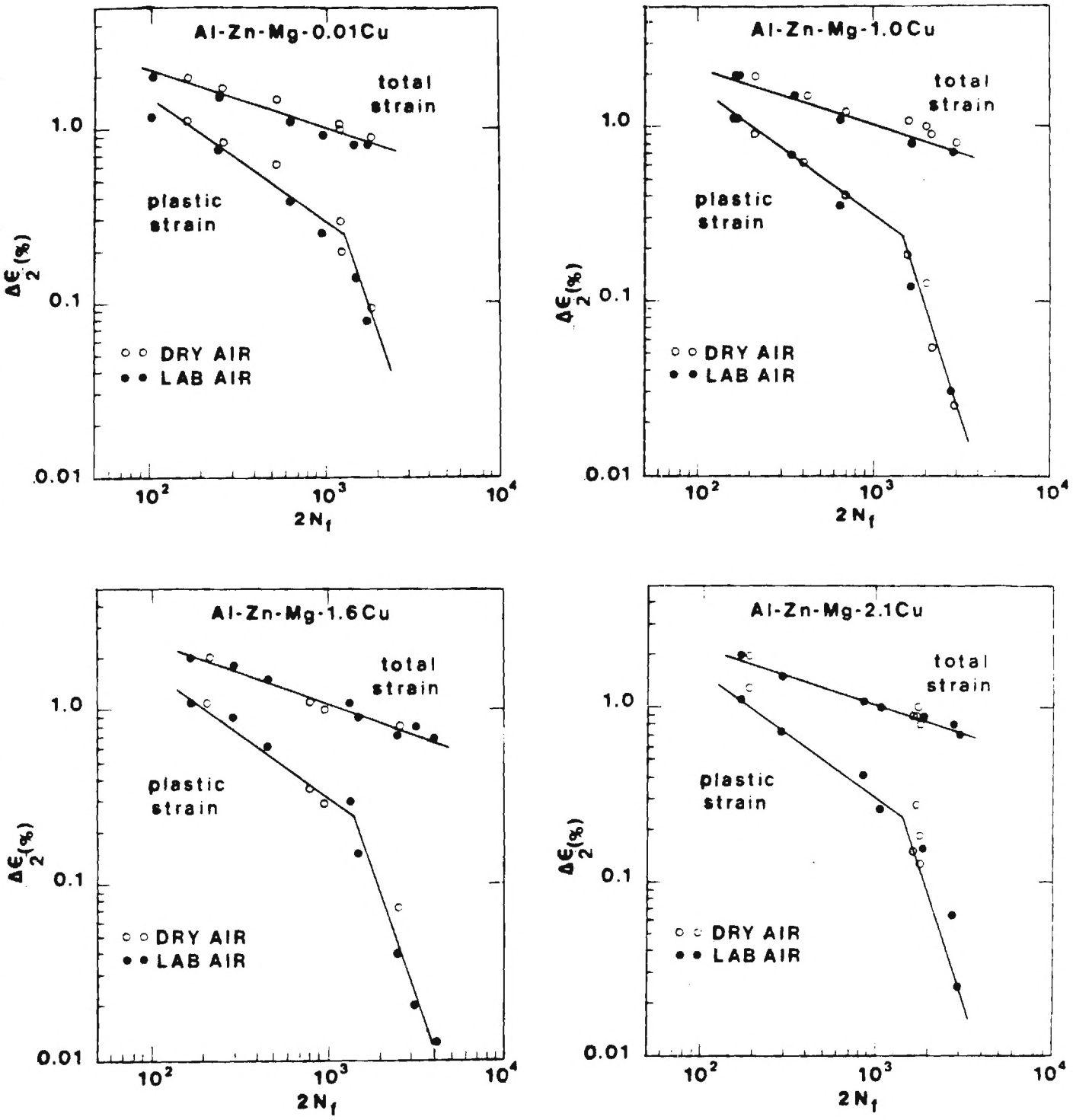

Figure 2. Strain-life (Coffin-Manson) curves of the four alloys tested in two environments.

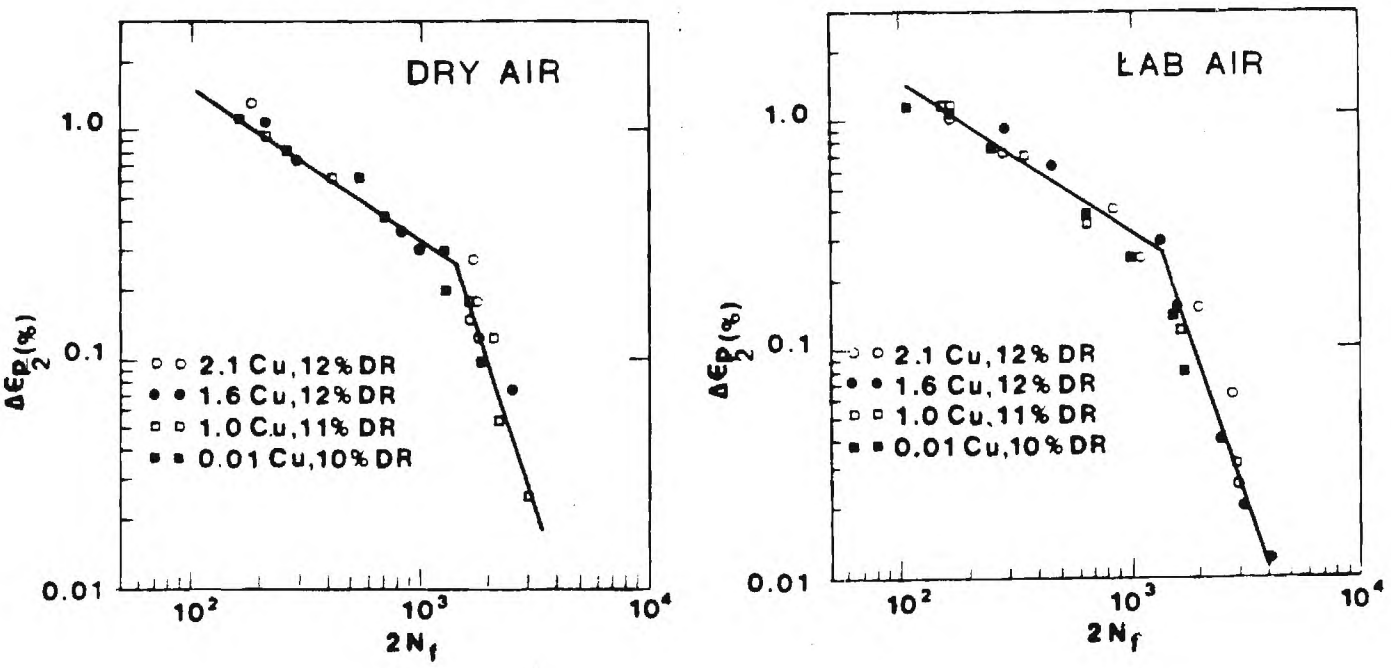

Figure 3. Superposition of the strain-life curves for the four Al-6Zn-2Mg-XCu alloys.

is accompanied by a more rapid decrease in the tensile stress than in the compressive stress since the crack closes during the compressive cycle. The plots of strain amplitude versus reversals to initiation also show a slope change, Fig. 4. Consequently, the slope change is not associated with changes in macroscopic crack propagation mechanism, but must be associated with changes in the initiation mechanism associated with changes in strain amplitude. It was noted earlier that cracks initiated at grain boundaries at high strain amplitudes and slip bands at low strain amplitudes. Strain localization within the PFZ is certainly a possibility in these overaged alloys, and its relationship to the observed phenomena is also being investigated.

2. FCP Behavior of Recrystallized Al-6Zn-2Mg-0.1Zr

The effect of aging treatment and environment on the fatigue crack growth rates of the Al-6Zn-2Mg-0.1Zr alloy is presented in Fig. 5. Growth rates of the underaged alloy tested in laboratory air, dry air and vacuum are lower than the da/dN values of the overaged alloy. The FCGR's of the underaged alloy increase in aggressive environments, especially at intermediate ranges of ΔK. Differences in crack propagation behavior for the two aging treatments can again be associated with deformation behavior.

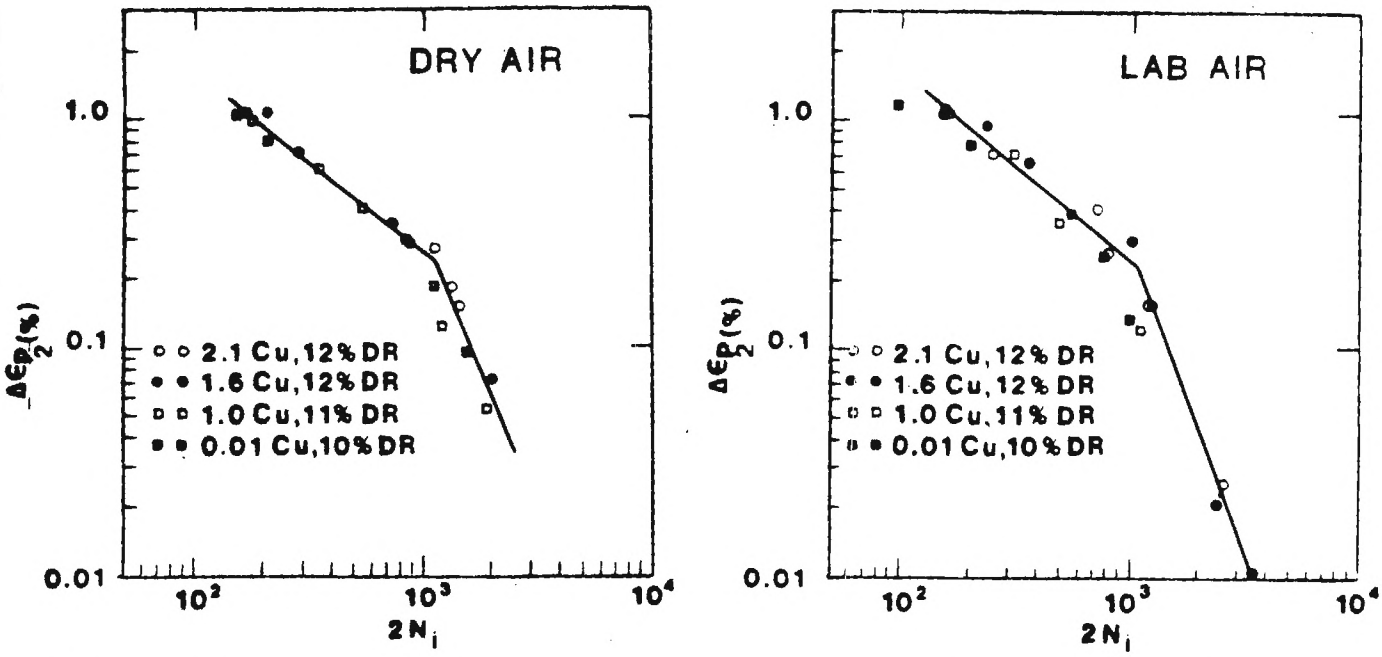

Figure 4. Plastic strain amplitude versus reversals to macroscopic crack initiation.

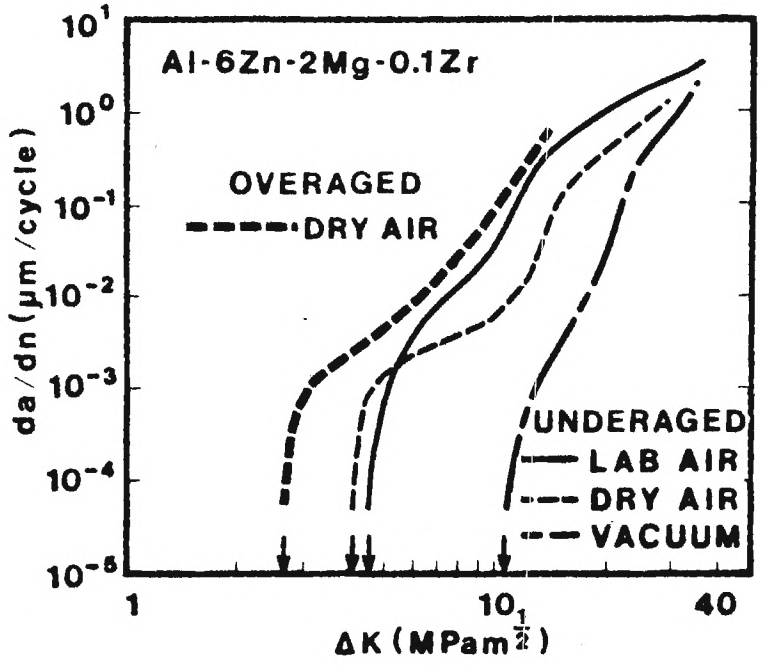

Figure 5. Effect of aging treatment and environment on the fatigue crack growth rate.

In the underaged condition, dislocation shearing of precipitates promotes coarse planar slip and inhomogeneous deformation which favor slip plane decohesion and the occurrence of zigzag growth and crack branching (12). Incoherent precipitates of overaged alloys are looped by dislocations, promoting more homogeneous slip, noncrystalline fracture and a single straight running crack which lies in a plane normal to the stress axis. The FCGR has been found to decrease (for any chosen calculated ΔK) as the fracture path changes from a single straight crack to a zigzag crack and then to a crack with numerous branches (12). Planar slip and inhomogeneous deformation enhances crack branching, increases the total crack path, and lowers the effective stress intensity at the tip of the crack. This lowers the fatigue crack growth rate. The slower FCGR of the underaged alloy may also be associated with a higher degree of slip reversibility (27).

An aggressive environment accelerates FCP over that in vacuum at equivalent values of ΔK, probably by reducing the amount of plasticity necessary for a particular increment of crack propagation (12). It may also be due to a decrease of both slip reversibility and the rewelding process. The latter is important since a considerable difference is observed in the FCGR between dry air and vacuum, Fig. 3. The environmental effect is probably associated with a form of hydrogen embrittlement in laboratory air. The exact mechanism of hydrogen embrittlement in aluminum alloys is still unknown, but it may be due to the combined action of a high pressure of hydrogen, a decrease of plasticity and a reduction of the cohesive strength of the lattice by adsorbed hydrogen. However, it is clear that the slip behavior affects the susceptibility to hydrogen embrittlement (28,29). When strain localization occurs more hydrogen atoms can be transported by dislocations moving in the localized slip bands, thereby increasing environmental sensitivity (12).

Eventually the FCP curves of samples tested in aggressive environments should converge to those of vacuum since at large ΔK plasticity effects dominate and occur too rapidly for chemical effects to be important. When this happens, there is a decrease in the slope of the FCP curve, as observed in Fig. 5.

3. Microstructure and Monotonic Properties of Two Al-3Li-2Cu-0.2Zr-XCd Alloys

The purpose of this study was to (a) investigate the effect of copper and zirconium on the strength and ductility of an aluminum alloy having a high lithium content, (b) determine the effect of cadmium on the recrystallization behavior of an alloy containing a strong recrystallization inhibitor like zirconium, and

(c) determine the effect of cadmium and stretching on the precipitation process during aging. The chemical compositions of the alloys studied are given in Table I.

TABLE I. CHEMICAL COMPOSITION OF THE ALLOYS, WT.%

	Li	Cu	Zr	Cd	Al
Alloy 1	2.7	2.3	.17	0	Bal
Alloy 2	2.7	2.3	.19	.19	Bal

3.1 Effect of Cd on the Recrystallization Behavior

The degree of recrystallization (DR) was determined after the various solutionizing treatments for both alloys. The Cd-free alloy did not recrystallize regardless of the solutionizing temperature. The unrecrystallized structure was very uniform and the unrecrystallized grains were composed of fine subgrains. TEM studies showed that the subgrain diameter varied from one to 10 μm. The 0.2% Cd alloy recrystallized either partially or totally, depending on the solutionizing temperature. For treatments below 763K, the alloy remained unrecrystallized. However, after solutionizing at 798K the structure consisted of large unrecrystallized regions, and large recrystallized regions; after solutionizing at 811K the unrecrystallized and recrystallized regions were intermixed on a finer scale; and after solutionizing at 823K, the structure was almost completely recrystallized (11). An unrecrystallized microstructure, similar to that obtained in the Cd-free alloy, was obtained in the Cd-containing alloy by preheating at 763K, prior to solutionizing at higher temperatures. The average DR through the whole cross section was determined to be 0, 39, 42, and 81% for the 763K, 798K, 811K and 823K solutionizing temperatures, respectively.

In order to determine the reason for the difference between the recrystallization behavior of the Cd-containing and Cd-free alloys, the microstructures of the extruded Cd-containing alloy, with or without preheat, were examined by transmission and scanning electron microscopy in conjunction with X-ray energy spectroscopy and compared with that of the Cd-free alloy. Similar studies were also done on alloys solutionized at 813K.

In the as-extruded condition, both alloys had a well defined subgrain structure and numerous large precipitates. In many cases, a high dislocation density was associated with these second phase particles. Two types of particles were present. One was $\sim$ 0.5 μm in size and XES analysis indicated that they contain an aluminum to copper ratio of $\sim$ 6:1. Although lithium cannot be detected by XES, the precipitate size, shape and the Al:Cu ratio suggest that they are the T_2 (Al_6CuLi_3) phase. The other precipitates were much larger ($\sim$5-10 μm) and had a much higher copper content (Cu:Al $\sim$ 1:2) and may be the T_B phase (30,31). The number density of this phase (henceforth called T_B) was similar for both alloys and the number density of T_2 was higher for the Cd-containing alloy. It appears that cadmium is a nucleating agent for T_2 during high temperature processing. When the extruded Cd-containing alloy was preheated to 763K, a significant reduction in the number density of the T_2 phase was observed. However, a very small change was observed in the number density of the T_B phase.

These T_B and T_2 phase particles, and associated deformation structure, may act as nucleating sites for recrystallization (32-35), and thus influence the recrystallization behavior. However, with the exception of some minor differences, this structure was present in both alloys and it is unlikely that the large difference observed in the recrystallization behavior can be solely due to such a small microstructural difference. Therefore, other factors which might influence the recrystallization behavior have to be considered, and the effect of zirconium was examined in this study.

The as-solutionized microstructure of the Cd-free alloy, and the Cd-containing alloy given the preheat, were essentially identical. Both contained a well defined subgrain structure and a much smaller volume fraction of the T_2 and T_B phase particles than observed in the as-extruded condition. Numerous small Al_3Zr precipitates were also observed. These small coherent precipitates are very effective in inhibiting recrystallization and grain growth. Rystad and Ryum (36) have suggested that the coherent nature of their interface imparts a high drag force on the recrystallization front since the precipitate/matrix interface has to change from coherent to semicoherent or incoherent as the recrystallization front passes the Al_3Zr precipitate.

X-ray energy spectroscopy indicated that some zirconium was present in the T_2 and T_B phases. However, for the Cd-containing alloy in the as-extruded condition, these phases also contained some cadmium and a much larger concentration of zirconium. The Cd-containing alloy preheated to 763K, not only

showed a significant reduction in the number of T_2 particles, but also showed a reduction in the zirconium concentration in the primary T_B phase. TEM studies on the as-extruded Cd-free alloy and the preheated Cd-containing alloy showed that both contained numerous Al_3Zr precipitates but the number density was smaller for the as-extruded Cd-containing alloy. Thus it appears that zirconium enters the larger precipitates if cadmium is present, but is released to form Al_3Zr during a preheat at 763K.

The influence that cadmium has on the recrystallization behavior of the Al-3Li-2Cu-0.2Zr alloy may simply be due to its tying up more of the zirconium in the T_2 and T_B phases and thus reducing the volume fraction of Al_3Zr. During the low temperature preheat most of the zirconium precipitates as Al_3Zr and recrystallization is suppressed during subsequent high temperature treatments. Although this interpretation may explain the present results, it does not explain why cadmium appears to enhance recrystallization in Zr-free alloys such as 2020. It is possible that the role of cadmium in nucleating large second phase particles may have a significant effect on recrystallization in these cases. Obviously, a more extensive study of this phenomenon would be of interest.

The variation of hardness with solutionizing temperature is shown in Fig. 6. The Cd-free alloy shows an increase in hardness with temperature up to 813K. This is an expected result, because the higher solutionizing temperature increases the solid solubility (reduces the amount of primary T_2 phase), which increases the amount of strengthening precipitates during subsequent aging. When the solutionizing temperature reaches about 813K it seems that most or all of the T_2 phase has been dissolved and a further increase in temperature has no discernible effect. A similar hardness behavior is also observed for the Cd-containing alloy when the alloy is given the preheat treatment discussed earlier. However, when solutionized without the preheat treatment, the hardness data appears erratic, Fig. 6. This behavior can be explained in terms of the mixed grain structure of the material as discussed previously. When the hardness measurement was made on the recrystallized area, a low value was obtained because of the loss of substructure strengthening in these regions.

3.2 Effect of Cadmium and Stretching on the Aging Behavior

For a given solutionizing and aging treatment, and identical grain structure, the hardness values of the Cd-free alloy always appears higher than those for the Cd-containing alloy, Fig. 6. The apparent reason for this behavior is that the presence of cadmium tends to stabilize the large T_2 precipitates thus removing some of the copper and lithium from forming the T_2 and δ' strengthening precipitates during aging.

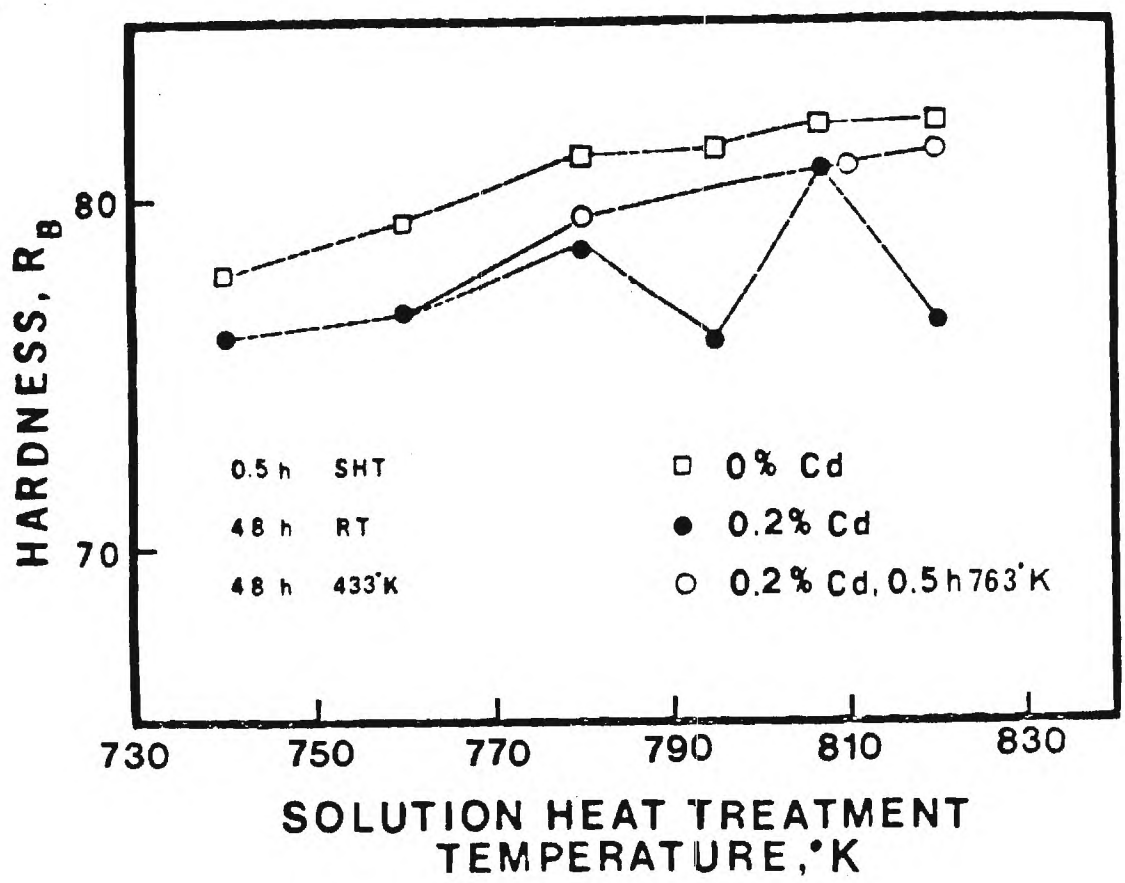

Figure 6. The effect of the SHT on the hardness of the alloy with 0% and 0.2% Cd.

TEM studies were conducted in order to determine the effect of cadmium and stretching on the precipitation behavior of the two alloys with a similar, unrecrystallized, grain structure. In the unstretched and aged condition, the Cd-containing alloy had more subgrain and grain boundary precipitates. Stretching prior to aging reduced the amount of subgrain and grain boundary precipitates. Energy dispersive analysis suggests that these precipitates are probably T_2 (Al_6CuLi_3).

Two types of matrix precipitates were detected, δ' (Al_3Li) and T_1 (Al_2CuLi). The platelet (or lathe) type precipitates were identified as T_1 and not θ' since they had a {111} habit plane which is the habit plane for T_1 (37). The habit plate of θ' is {100} (38,39). In the unstretched condition, the T_1 precipitates were observed either on low angle (subgrain boundaries or in isolated areas within the grains (most likely on dislocations). The Cd-containing alloy did not appear to have more T_1 than the Cd-free alloys. Al_3Li PFZ's were not observed around some of the subgrain boundaries that were free of the large precipitates.

Stretching prior to aging seems to reduce the amount of subgrain boundary precipitation for both alloys. However, no significant change in the δ' PFZ was observed. Stretching greatly increases the amount of T_1 precipitation within the matrix and the PFZ for T_1 appears to be smaller than that for δ'. In fact, the T_1 lathe spacing appears to be as large or larger than the distance between the grain boundaries and the nearest T_1 precipitates. Cadmium does not appear to significantly influence the precipitation behavior of the stretched alloys.

3.3 Tensile Properties

The tensile properties for the two alloys in the unrecrystallized condition are given in Table II. The Cd-containing alloy has a slightly higher yield strength in the as-quenched condition; however, the yield strength is either equal to or slightly lower than the Cd-free alloy for aging times up to and including 16h at 463K. The yield strength is somewhat lower in the overaged condition (by 46 MPa) and the stretched and 16h aged condition (by 30 MPa). Since cadmium atoms have a high binding energy with vacancies (40) they may act as a vacancy pump (41,42) in the late stages and thus accelerate the overaging effects. The presence of cadmium does not seem to induce the same positive effect on precipitation of these high Li:Cu ratio alloys as it does on low Li:Cu ratio alloys. This confirms the earlier suggestion by Silcock (31) that cadmium has a significant effect on the nucleation of θ' but only a minor effect on the nucleation of T_1.

The elongation to fracture dropped off sharply with the initial aging step and remained relatively constant as aging progressed. Neither the presence of cadmium nor the stretching treatment significantly affect the ductility; however, the highest strength was obtained for the stretched and aged alloys. The effect of DR on the tensile properties is shown in Table III. The yield strength decreases with DR; probably due to a loss in substructure strengthening. There appears to be a small increase in elongation with increase in DR.

3.4 Summary of Al-3Li-2Cu-0.2Zr-XCd Research

Cadmium has a significant effect on the recrystallization behavior of Al-Li-Cu-Zr alloys. It appears to tie up some of the zirconium during high temperature processing and thus reduce the volume fraction of the recrystallization-inhibiting precipitate Al_3Zr. Cadmium does not aid in the precipitation of the strengthening precipitates T_1 and δ' in the Al-3Li-2Cu-0.2Zr alloy. It has a detrimental effect since it combines with copper and lithium in the form of coarse grain boundary precipitates thus reducing the amount of these elements participating in the aging treatment. A stretch prior to natural and artificial

TABLE II. TENSILE PROPERTIES

	0% Cd Unrecrystallized			0.2% Cd Unrecrystallized		
Aging	$\sigma_{0.2}$ MPa (ksi)	σ_{uts} MPa (ksi)	ε_f%	$\sigma_{0.2}$ MPa (ksi)	σ_{uts} MPa (ksi)	ε_f%
As quenched	179 (26)	392 (57)	15.2	192 (28)	384 (56)	16.2
3 h @ 463°K	424 (62)	528 (77)	5.2	422 (62)	510 (74)	4.3
10 h @ 463°K	472 (69)	558 (81)	3.6	447 (65)	528 (77)	3.6
16 h @ 463°K	445 (65)	552 (81)	5.7	441 (64)	556 (81)	5.5
48 h @ 463°K	440 (64)	538 (79)	5.8	394 (58)	496 (72)	5.6
2% stretch + 16 h @ 463°K	503 (73)	561 (82)	4.0	473 (69)	550 (80)	4.2

TABLE III. EFFECTS OF DR ON THE TENSILE PROPERTIES OF Al-3Li-2Cu-0.3Zr-0.2Cd

DR in Gage Section %	$\sigma_{0.2}$ MPa (ksi) aged 16h @ 463°K	σ_{uts} MPa (ksi)	ε_f%
0	441 (64)	556 (81)	5.5
27	416 (61)	524 (77)	5.5
60	373 (54)	493 (72)	6.9
60*	426 (62)	517 (75)	7.0

* Given 1% stretch prior to aging.

aging increases the strength with no significant loss in ductility. The dislocations generated by the stretch act as nucleating sites for the T_1 precipitates. The low ductility observed for these alloys in the aged conditions is most likely associated with strain localization either in coarse slip bands or in PFZ's.

C. PLANS FOR REMAINING MONTHS OF CONTRACT PERIOD

1. Al-Zn-Mg Alloys

We are now completing a study on the relationship between microstructure, cyclic stress strain response and fatigue crack propagation of an Al-6Zn-2Mg-0.2Zr alloy. Intermediate thermal mechanical processing has been used to obtain a completely recrystallized, fine grain structure. Measurements are being made in vacuum to minimize environmental effects and on the alloy in the underaged condition to minimize PFZ effects. The slip length is determined by the grain size since the strengthening precipitates are coherent and sheared by dislocations, which enhances planar slip. This alloy and heat treatment thus allows an evaluation of the effects of slip length, cyclic flow stress and ductility on the fatigue crack propagation behavior. The fatigue crack growth measurements have been completed and the low cycle fatigue measurements are scheduled for the last week in August. The vacuum LCF measurements will be made at the University of Pennsylvania in Professor Cambell Laird's laboratory in order to meet the time table of this contract. Once the cyclic stress strain parameters have been measured they will be used in conjunction with microstructural data to calculate fatigue crack growth rates. The experimental fatigue crack growth rates will be compared

with those calculated using the model developed in our laboratory by Chakrabortty(43). The Chakrabortty model uses a ductility exhaustion mechanism and calculates the fatigue crack growth rate from LCF properties and slip length. The crack growth rate equation obtained from the model does not contain any adjustable parameters which allows a direct comparison with experimental measurements. Once experimental verification of the model has been established, it can be used in the design of alloys for fatigue resistance.

2. Al-Li-X Alloys

We are now in the process of determining the effect of slip distribution on the monotonic and cyclic ductility of a series of Al-Li binary alloys. The primary phenomena which appear to dominate the ductility and fracture characteristics in precipitation hardening Al-Li alloys is the tendency toward strain localization. The shearable nature of the precipitates tends to localize the strain in intense bands of deformation which act as stress concentrations at grain boundary triple junctions. Cracks can then nucleate at these triple junctions and propagate intergranularly. On the other hand, strain localization can occur in the PFZ's and cracks can then nucleate at grain boundary precipitates and propagate intergranularly within the PFZ. The goal of this phase of our program is to understand the influence of lithium content on the distribution of deformation and the influence of that distribution on monotonic and cyclic ductility. The lithium composition was selected to examine the effect of lithium in: (1) a solid solution containing short range order (Al-0.9%Li); (2) a two phase alloy having a small volume fraction of δ' (Al-1.5%Li); and (3) a two phase alloy having a large volume fraction of δ'. Monotonic and cyclic tests of these alloys have been completed. During the remainder of this year, we plan to evaluate the results and prepare a manuscript for publication.

III. PROPOSED RESEARCH

A. EXPERIMENTAL

1. Improvement in the Ductility of High Strength Al-Li Alloys by Thermal Mechanical Treatments

The grain size and shape, degree of recrystallization and crystallographic texture can greatly effect the properties of aluminum alloys (1,7,8,11,23,43,45). Intermediate thermal mechanical treatments (ITMT) of commercial, ingot metallurgy aluminum alloys have resulted in refined grain structures (23,45-49), modified particle distributions (48), and changes in crystallographic texture (23,45). The first ITMT processing, designated as ISML-ITMT, included partial homogenization, relatively low temperature working, recrystallization and homogenization. A recrystallized, fine, equiaxed grain structure was developed for 7075. According to DiRusso et al. (46), the success of the ISML-ITMT process was based on making Cr ineffective in retarding the recrystallization of worked ingot into a fine grain structure. Most of the CR was retained in supersaturated solid solution during the low temperature working stage. Waldman et al. (48) suggested that the recrystallization was due to the suppression of dynamic recovery by the introduction of a high degree of strain energy at a relatively low temperature. A later process, designated FA-ITMT, involved the use of several homogenization treatments to precipitate Cr, Zn, Mg and Cu as coarse particles. A large dislocation density was then generated at these particles by warm working. Recrystallization was then sufficiently activated to proceed during a subsequent anneal. This process produced the same microstructure and tensile properties as those of the ISML-ITMT processed 7075 alloys. A recent study (49) indicated that particles (dispersoids and overaged precipitates) larger than 0.75 μm can act as preferential nucleation sites for recrystallizing grains. A correlation was noted between the number of particles capable of providing nucleation sites for recrystallization and the size of the recrystallized grains. It should, therefore, be possible to obtain a desired grain size by manipulating the size and distribution of these particles.

Microstructures may effect mechanical and stress-corrosion properties in a different manner. It has been shown that smaller grain size, which has a beneficial effect on resistance to fatigue crack initiation, may have a detrimental effect on fatigue crack propagation resistance. Grain character (size, shape, distribution and texture) plays an important role in deformation and fracture--in both the initiation and propagation behavior. This role may change with variations in the matrix precipitate, applied load and environment.

Therefore, an optimization is necessary to acquire the right microstructure for a given product and application.

Recent studies at Georgia Tech showed that the Al-Cu-Li alloy 2020-T651 plate, which was partially recrystallized with large recrystallized grains (975 μm along the rolling direction), exhibited 5.0 and 2.2% elongation in longitudinal and long transverse direction, respectively. This low ductility is believed to be associated with strain localization compounded by the large grain size. Consequently, improvement in the properties of the 2020 alloy may be obtained by modifications of the grain structure which reduce the slip distance and decrease strain localization.

This phase of our research program is directed toward improving the ductility of Al-Li alloys, such as 2020, by control of the grain structure through ITMT. This work includes developing: (1) completely recrystallized grain structures with different grain sizes, (2) partially recrystallized grain structures with different degrees of recrystallization, and (3) completely unrecrystallized structures with different unrecrystallized grain sizes. The results of this systematic study should elucidate the influence of grain structure on the ductility of commercial-type Al-Li alloys that are subject to extensive strain localization. They should also provide a basis for improving the ductility of 2020 and similar alloys through grain structure control.

2. The Effect of Microstructure on the Corrosion and Stress Corrosion Cracking Resistance of High Strength Al-Li Alloys

The objective of this study is to characterize the stress corrosion resistance and electrochemical behavior of aluminum alloy 2020. The major emphasis will be on the relationship between stress corrosion resistance and the variation of microstructure with heat treatment. Although many Al-Li-X alloys have been and are being studied, alloy 2020 was chosen for this research program because it was once commercially available and because of its superiority in specific strength and specific modulus over 2024 and 7075, which currently predominate in aircraft structural applications. Obviously, if its ductility can be enhanced with little or no sacrifice in strength, 2020 would be an extremely attractive aerospace alloy. A recent study (50) has shown that tensile ductility and fracture toughness can be substantially improved, with a small sacrifice in strength, through an underaging treatment. However, for many commercial applications, the extent to which the mechanical properties

can be exploited depends on a thorough knowledge of stress corrosion resistance, and date adequate for design purposes are not available for this alloy. During the time 2020 was being commercially produced (1959-1969), it was summarily reported that, in the peak aged condition, its corrosion resistance was adequate and its stress corrosion resistance was good, but no specific data were cited. Of course, no data are yet available for the higher toughness, underaged condition.

The primary goals of this study are to fill the void of information by determining the corrosion and stress corrosion behavior of 2020 as a function of the microstructural changes produced by aging and to interpret this data in relation to the existing models for SCC of aluminum alloys.

2.1 Material Characterization

All specimens for this work will be cut from a single piece of commercially produced 2020 plate, one inch thick. This material was obtained from the Air Force Materials Laboratory and was in the T651 condition, as received. The chemical analysis, in weight percent, is given below:

Cu	Li	Cd	Mn	Si	Fe	Zn	Ti	Al
4.45	1.21	0.21	0.51	0.08	0.16	0.04	0.06	Balance

A preliminary investigation has been made, in which the response of the alloy to isothermal precipitation hardening treatments at 137°, 149°, and 160°C (279°, 300°, and 320°F) was determined. This tempering range has been previously shown to produce maximum strength. The precipitation hardening procedure to be used in the present study is as follows: solution heat treat for at least 1.5 hours in an inhibited molten salt bath, cold water quench, store at room temperature for 7-14 days, and isothermally age at 149°C (300°F) for various times to obtain a range of mechanical/microstructural properties.

Tensile properties will be determined for various heat treatments, using duplicate samples of longitudinal orientation. Fracture toughness will be estimated using double cantilever beam samples designed for stress corrosion crack propagation tests. While this will not constitute a rigorous K_{I_C} determination, it should be sufficiently close for the present characterization purposes.

The changes in the microstructure with aging will be studied using transmission electron microscopy (TEM), and the correlation of microstructure with mechanical properties will be determined. Deformation characteristics will be examined, using TEM samples taken from the tensile specimens. The effects of microstructural variations upon corrosion behavior and stress corrosion susceptibility will be studied in detail.

2.2 Corrosion Behavior

The electrochemical behavior of alloy 2020 in 3.5% aqueous sodium chloride solution will be analyzed, using polarization techniques and electrode potential measurements. The changes in free corrosion potential as a function of isothermal aging time will also be determined. Variations of polarization parameter with aging will also be investigated and correlations with microstructural changes will be sought. Surface degradation occurring during these corrosion tests will be studied, using optical metallography and scanning electron microscopy (SEM). An investigation of corrosion attack on the microscopic scale will be attempted. Discs for TEM foil preparation will be exposed to a corrosive environment, then thinned by electropolishing from one side, so that the attack on the surface masked during polishing will be preserved for TEM examination.

2.3 Stress Corrosion Cracking

Stress corrosion cracking characteristics of the 2020 plate in 3.5% sodium chloride solution will be determined using a variety of techniques. The primary effort will employ double cantilever beam (DCB), constant crack opening displacement samples, described by Sprowls (51). These samples will be of short transverse orientation, chevron notched and fatigue pre-cracked. K_Q values will be determined for some samples, after a short fatigue crack has been introduced. For these samples, following measurement of the stress intensity at pop-in, further fatigue pre-cracking will be done to move the crack tip beyond the plastic zone created by the K_Q test. Stressing to the desired level for SCC testing will be done on the tensile machine used for pre-cracking and the constant crack opening displacement will be maintained by placing a wedge of 2020 in the notch, at or near the pre-cracking load line. The corrodent will be introduced immediately after stressing and the crack will be sealed with a transparent film to prevent leakage, yet allow crack growth to be visually monitored. Knowledge of the variation of stress intensity with crack length at constant crack opening displacement will allow the determination of crack velocity versus stress intensity. Plateau velocities will be measured for peak aged material and several underaged conditions. Some values for crack velocity in the stress intensity dependent region will also be determined.

2.4 Fractography

Fractographic studies will be made on fractured DCB and U-bend specimens, with emphasis on fracture mode, particles associated with the fracture surface, and apparent corrosion damage. Metallography of stopped cracks as well as SEM and microprobe analysis of fracture surfaces will be used.

2.5 Crack Solution Chemistry

As part of an investigation currently in progress concerning solution chemistry in stress corrosion cracks, the changes in solution pH and potential will be monitored for some of the DCB samples, using embedded micro-electrodes. Also, a previously developed freeze drying technique will be used to study chemical changes in the solution, especially dissolved ions from the crack surfaces.

2.6 Preliminary Discussion

In addition to providing valuable information on the stress corrosion resistance and electrochemical behavior of alloy 2020, it is expected that this study will contribute to the overall understanding of SCC of aluminum alloys. The results will be analyzed with respect to the existing models for stress corrosion cracking.

Since 2020 was discontinued because of its low ductility and low fracture toughness, reconsideration of this alloy or a similar composition would necessitate a substantial improvement in these properties. Sanders (50) has shown that an underaging treatment can significantly improve the ductility and toughness of 2020. It has also been demonstrated that underaging yields greater toughness than overaging to the same strength level, for alloy 2014 (52). However, it has been reported (53) that underaging decreases the resistance of Al-Cu alloys to corrosion and SCC. The details of a compromise between toughness and SCC resistance will be determined in this study.

3. Trace Element and Interactive Effects of Alloy Additions in Al-Li Alloys

In many cases the presence of minor alloying additions in age hardening alloys such as Al-Li can greatly affect the precipitation and subsequent coarsening of the strengthening precipitates. Although the effect of trace elements is not amenable to a single explanation, the models of Nickolson (54,55) and Pashley (56) are sufficient to encompass their role in the decomposition process. Nicholson (57) and Palmear (58) have summarized possible effects of trace additions by suggesting that they can modify the precipitation process by:

(a) interaction with vacancies,

(b) controlling the dislocation density that might be produced by annihilation of vacancies,

(c) raising or lowering the critical temperature for homogeneous decomposition,

(d) changing the interface energy of the clusters and/or precipitates (this affects both nucleation and coarsening of the precipitates),

(e) altering the type of precipitate formed,

(f) forming insoluble particles which in turn modify the grain size and shape rather than the aging process,

(g) segregating to grain boundaries and inhibiting discontinuous precipitation.

Starke (59) has reviewed the work on trace element additions to Al-base alloys that was completed prior to 1970. Of particular interest to the current program, is the effect of trace additions (or third element additions) to Al-Li alloys. Earlier work showed that additions of copper together with small additions of cadmium, considerably increase the strength of Al-Li alloys with no corresponding decrease in ductility (60,61). Cadmium has been shown to facilitate the precipitation of θ' in Al-Cu alloys (62-64) and was added to 2020 for that purpose Cadmium may also aid in the formation of the T_1 (Al_2CuLi) and T_2 (Al_6CuLi_3) phases in Al-Li-Cu alloys (60).

The recent study by Lin, Chakrabortty and Starke (65) (see Section II-2) on the effect of cadmium additions to an Al-3Li-2Cu-0.2Zr alloy showed that cadmium has a significant effect on the recrystallization behavior of Al-Li-Cu-Zr alloys. It appears to tie up some of the zirconium during high temperature processing and thus reduce the volume fraction of the recrystallization--inhibiting precipitate Al_3Zr. Cadmium does not aid in the precipitation of the strengthening precipitates T_1 and δ' in the Al-3Li-2cu-0.2Zr alloy. It has a detrimental effect since it combines with copper and lithium in the form of coarse grain boundary precipitates thus reducing the amount of these elements participating in the aging treatment. This example illustrates that trace elements can greatly influence the microstructure and related properties of Al-Li alloys and the effect is sensitive to alloy content and primary processing parameters. Cadmium aided in the precipitation of the strengthening precipitates in the high copper low lithium alloy 2020, but did not have this beneficial effect for the high lithium low copper alloy. It should also be mentioned that cadmium may also have a detrimental effect on 2020 by enhancing recrystallization and subsequent grain growth (66,67). As mentioned in the previous sections, the large recrystallized grains in conjunction with strain localization may be partly responsible for the low ductility and fracture toughness in 2020.

The research described above illustrate the importance of trace element additions, and interactive effects of alloying elements, on the microstructure and properties of Al-Li alloys. We propose to continue our work in this area during the coming year. Since one of the problems associated with Al-Li alloys

involves extensive strain localization due to the lack of interfacial strain associated with the Al_3Li precipitate, next year's program will consider trace element additions selected to change the coherency strain field and interfacial energy of the Al_3Li phase.

B. WORK STATEMENT

The primary objectives of the proposed research are to establish the effects of (a) alloy chemistry, (b) microstructure, (c) deformation mode, and (d) environment on the monotonic and cyclic properties of high strength aluminum alloys. The research planned for the coming year concentrates on the Al-Li-X system. Aluminum-lithium alloys offer a combination of high elastic modulus and low density, properties which are desired for high performance aircraft. To meet the objectives of program, we have selected special alloys and heat treatments designed to separate the various metallurgical variables, and propose to make property measurements which will establish microstructure-environment-property relationships. The measurements, which include tensile, fracture toughness, low-cycle and high cycle fatigue, and crack propagation, will be made in both inert and aggressive environments.

THE EFFECT OF MICROSTRUCTURE ON THE PROPERTIES OF HIGH STRENGTH ALUMINUM ALLOYS

AFOSR Annual Scientific Report
February 1982

by

Edgar A. Starke, Jr. and F. S. Lin
Fracture and Fatigue Research Laboratory
Georgia Institute of Technology
Atlanta, Georgia 30332

This research was sponsored by the Air Force Office of Scientific Research Directorate of Electronics and Solid State Sciences under Research Grant Number AFOSR-78-3471

unclassified

SECURITY CLASSIFICATION OF THIS PAGE (When Data Entered)

REPORT DOCUMENTATION PAGE		READ INSTRUCTIONS BEFORE COMPLETING FORM
1. REPORT NUMBER	2. GOVT ACCESSION NO.	3. RECIPIENT'S CATALOG NUMBER
4. TITLE (and Subtitle) THE EFFECT OF MICROSTRUCTURE ON THE PROPERTIES OF HIGH STRENGTH ALUMINUM ALLOYS		5. TYPE OF REPORT & PERIOD COVERED Annual 1/1/81 - 12/31/81 6. PERFORMING ORG. REPORT NUMBER E-19-636-81 Annual
7. AUTHOR(s) Edgar A. Starke Jr and F. S. Lin		8. CONTRACT OR GRANT NUMBER(s) AFOSR-78-3471
9. PERFORMING ORGANIZATION NAME AND ADDRESS Fracture & Fatigue Research Laboratory Georgia Institute of Technology Atlanta, GA 30332		10. PROGRAM ELEMENT, PROJECT, TASK AREA & WORK UNIT NUMBERS
11. CONTROLLING OFFICE NAME AND ADDRESS Air Force Office of Scientific Research Directorate Electronics and Solid State Sciences Bolling AFB, Washington DC 20332		12. REPORT DATE Feb 25, 1982 13. NUMBER OF PAGES 47
14. MONITORING AGENCY NAME & ADDRESS(if different from Controlling Office)		15. SECURITY CLASS. (of this report) unclassified 15a. DECLASSIFICATION/DOWNGRADING SCHEDULE

16. DISTRIBUTION STATEMENT (of this Report)

unlimited

17. DISTRIBUTION STATEMENT (of the abstract entered in Block 20, if different from Report)

18. SUPPLEMENTARY NOTES

19. KEY WORDS (Continue on reverse side if necessary and identify by block number)

Aluminum alloys, microstructure

20. ABSTRACT (Continue on reverse side if necessary and identify by block number)

This program was initiated in January, 1978, and is concerned with the effect of microstructure on the properties of two different classes of aluminum alloys of current interest to the Air Force: (1) high strength Al-Zn-Mg-X alloys and (2) low density, high modulus Al-Li-X alloys. Progress during 1981 may be summarized as follows:

(1) Al-Zn-Mg-X Alloys: The low cycle fatigue (LCF) and fatigue crack propagation (FCP) behavior of an Al-6Zn-2Mg-0.1Zr alloy was studied in various environments for two different aging treatments. Strain-life curves indicate the

DD FORM 1 JAN 73 1473 EDITION OF 1 NOV 65 IS OBSOLETE

unclassified

SECURITY CLASSIFICATION OF THIS PAGE (When Data Entered)

fatigue crack initiation resistance of the alloy in the overaged condition is considerably greater than that in the underaged condition. In addition, a comparison of the curves for both aged conditions shows that the LCF resistance of the underaged alloy is significantly affected by environment but the LCF resistance of the overaged alloy is environmentally insensitive. These differences have been related to changes in deformation behavior.

The underaged alloy exhibits a lower fatigue crack growth rate (FCGR) than that of the overaged alloy. Growth rates increase in aggressive environments for the underaged alloy with the effect being most noticeable at intermediate ranges of ΔK. The shape of the growth rate curves is correlated with transitions in the fracture surface appearance which is controlled by the deformation behavior.

Comparisons between experimental and predicted FCGR's using the Chakrabortty equation showed excellent agreement at high ΔK. However, the predicted FCGR gradually begins to overestimate the measured data with decreasing ΔK. This difference is attributed to closure and threshold effects. The experimentally measured FCGR has been replotted as a function of ΔK_{eff} to account for closure and the Chakrabortty program has been modified relating ΔK_{th} with a critical strain, $\Delta\varepsilon_{pth}$, below which cracks cease to propagate. Those modifications resulted in excellent agreement between the predicted and experimental crack growth curves over the entire range of ΔK.

(2) Al-Li-X Alloys: The monotonic and cyclic properties of three Al-Li alloys were correlated with the slip behavior. One alloy was a solid solution with short range order, one had a small volume fraction of shearable precipitates, and one had a large volume fraction of shearable precipitates. Both the monotonic and cyclic ductility were controlled by the degree of strain localization which depended on the extent of work softening on the glide plane. When a large volume fraction of precipitates were present, cracks nucleated at grain boundary ledges during tensile tests and propagated either transgranularly or intergranularly along precipitate free zones. The propagation mechanism depended on the aging treatment. Cracks most often nucleated at slip bands during cyclic deformation, and propagated either by the striated growth mechanism or by slip band decohesion; the path contingent on the extent of strain localization.

The microstructure and tensile properties of two Al-3wt.%Li-2wt.%Cu-0.2wt.%Zr alloys, one Cd-free and one containing 0.2wt.%Cd, have also been investigated. The Cd-free alloy remained unrecrystallized for all solutionizing treatments studied; whereas a special treatment had to be developed to prevent recrystallization during solutionizing of the 0.2wt.%Cd alloy. In combination with cadmium, zirconium either enters into, or nucleates on, the coarse Al_7Cu_2Fe and T_2 phases during high temperature annealing. This reduces the volume fraction of small coherent Al_3Zr particles in the matrix which normally inhibits recrystallization. Consequently, a low temperature anneal to precipitate Al_3Zr is necessary prior to high temperature solutionizing in order to prevent recrystallization in the Cd-containing alloy. Unlike its effect in lower lithium, higher copper content aluminum alloys, cadmium does not significantly affect the nucleation of the strengthening precipitates. If anything, cadmium has a detrimental effect on the age hardening response of this alloy since it increases the formation of coarse Al-Cu-Li equilibrium phases at grain and subgrain boundaries and thus removes some of the copper and lithium from participating in the formation of the strengthening precipitates T_1 and δ'. Subgrain boundary fracture occurred during tensile tests of both alloys in the unrecrystallized condition; however, transgranular fracture occurred in tests of the partially recrystallized 0.2wt.%Cd alloy. Both types of fractures are believed due to a form of strain localization associated with precipitate free zones and shearable precipitates.

END

TABLE OF CONTENTS

ABSTRACT

This program was initiated in January, 1978, and is concerned with the effect of microstructure on the properties of two different classes of aluminum alloys of current interest to the Air Force: (1) high strength Al-Zn-Mg-X alloys and (2) low density, high modulus Al-Li-X alloys. Progress during 1981 may be summarized as follows:

(1) Al-Zn-Mg-X Alloys

The low cycle fatigue (LCF)and fatigue crack propagation (FCP) behavior of an Al-6Zn-2Mg-0.1Zr alloy was studied in various environments for two different aging treatments. Strain-life curves indicate the fatigue crack initiation resistance of the alloy in the overaged condition is considerably greater than that in the underaged condition. In addition, a comparison of the curves for both aged conditions shows that the LCF resistance of the underaged alloy is significantly affected by environment but the LCF resistance of the overaged alloy is environmentally insensitive. These differences have been related to changes in deformation behavior.

The underaged alloy exhibits a lower fatigue crack growth rate (FCGR) than that of the overaged alloy. Growth rates increase in aggressive environments for the underaged alloy with the effect being most noticeable at intermediate ranges of ΔK. The shape of the growth rate curves is correlated with transitions in the fracture surface appearance which is controlled by the deformation behavior.

Comparisons between experimental and predicted FCGR's using the Chakrabortty equation showed excellent agreement at high ΔK. However, the predicted FCGR gradually begins to overestimate the measured data with decreasing ΔK. This difference is attributed to closure and threshold effects. The experimentally measured FCGR has been replotted as a function of ΔK_{eff} to account for closure

and the Chakrabortty program has been modified relating ΔK_{th} with a critical strain, $\Delta\varepsilon_{p_{th}}$, below which cracks cease to propagate. Those modifications resulted in excellent agreement between the predicted and experimental crack growth curves over the entire range of ΔK.

(2) Al-Li-X Alloys

The monotonic and cyclic properties of three Al-Li alloys were correlated with the slip behavior. One alloy was a solid solution with short range order, one had a small volume fraction of shearable precipitates, and one had a large volume fraction of shearable precipitates. Both the monotonic and cyclic ductility were controlled by the degree of strain localization which depended on the extent of work softening on the glide plane. When a large volume fraction of precipitates were present, cracks nucleated at grain boundary ledges during tensile tests and propagated either transgranularly or intergranularly along precipitate free zones. The propagation mechanism depended on the aging treatment. Cracks most often nucleated at slip bands during cyclic deformation, and propagated either by the striated growth mechanism or by slip band decohesion; the path contingent on the extent of strain localization.

The microstructure and tensile properties of two Al-3wt.%Li-2wt.%Cu-0.2wt.%Zr alloys, one Cd-free and one containing 0.2wt.%Cd, have also been investigated. The Cd-free alloy remained unrecrystallized for all solutionizing treatments studied; whereas a special treatment had to be developed to prevent recrystallization during solutionizing of the 0.2wt.%Cd alloy. In combination with cadmium, zirconium either enters into, or nucleates on, the coarse Al_7Cu_2Fe and T_2 phases during high temperature annealing. This reduces the volume fraction of small coherent Al_3Zr particles in the matrix which normally inhibits recrystallization. Consequently, a low temperature anneal to precipitate Al_3Zr is necessary prior to high temperature solutionizing in order to prevent recrys-

tallization in the Cd-containing alloy. Unlike its effect in lower lithium, higher copper content aluminum alloys, cadmium does not significantly affect the nucleation of the strengthening precipitates. If anything, cadmium has a detrimental effect on the age hardening response of this alloy since it increases the formation of coarse Al-Cu-Li equilibrium phases at grain and subgrain boundaries and thus removes some of the copper and lithium from participating in the formation of the strengthening precipitates T_1 and δ'. Subgrain boundary fracture occurred during tensile tests of both alloys in the unrecrystallized condition; however, transgranular fracture occurred in tests of the partially recrystallized 0.2wt.%Cd alloy. Both types of fractures are believed due to a form of strain localization associated with precipitate free zones and shearable precipitates.

I. THE EFFECT OF ENVIRONMENT ON THE LOW CYCLE FATIGUE LIFE AND FATIGUE CRACK PROPAGATION BEHAVIOR OF AN Al-6Zn-2Mg-0.1Zr ALLOY (Heikkenen, Lin, and Starke)

Many structural materials fail by corrosion fatigue if they are exposed to an aggressive environment while undergoing cyclic loading. It is apparent that the consideration of corrosion fatigue characteristics associated with the intended service environment is a primary factor in evaluating and selecting materials which resist fatigue cracking. The corrosion fatigue behavior is controlled by microstructural features which control deformation processes. In order to improve the resistance to corrosion fatigue cracking, we must determine the parameters that control the process and whether or not they can be modified by metallurgical manipulations. Care should be exercised when drawing conclusions from fatigue studies. Microstructural features that raise the resistance to crack initiation may lower the resistance to crack propagation, and vice versa. Consequently, it is absolutely necessary to correlate microstructure with the fatigue property of interest so that such a distinction can be made.

The aim of this task was to characterize the effect of environment on the low cycle fatigue life and fatigue crack propagation behavior of an Al-6Zn-2Mg-0.1Zr alloy. Specimens were examined in both an underaged and overaged condition in order to evaluate the environmental sensitivity of the different heat treatments.

STRAIN-LIFE BEHAVIOR

Since fatigue damage is caused by cyclic plastic strain, the fatigue life may be related to the plastic strain amplitude. Figure 1 shows the effect of aging treatment on the LCF behavior of the Al-6Zn-2Mg-0.1Zr alloy tested in laboratory air and dry air. The LCF resistance of the overaged alloy was considerably greater than that of the underaged alloy. These differences in the strain-life behavior can be associated with changes in deformation behavior. Shearable precipitates of the underaged alloy enhance planar slip and strain localization, resulting in coarse planar slip and large surface offsets. This

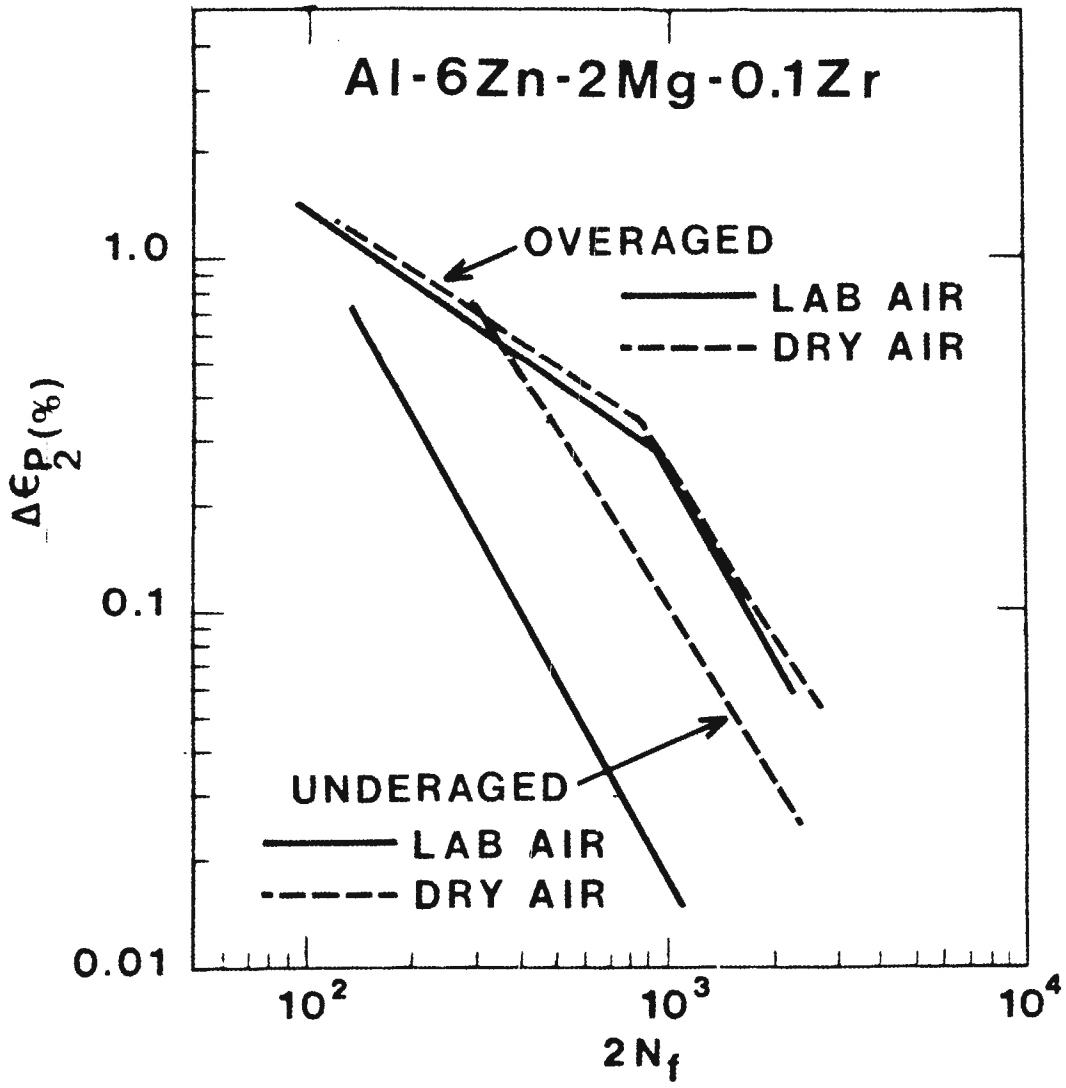

FIGURE 1. Effect of aging treatment on the LCF behavior; tests conducted in laboratory and dry air environments.

leads to early crack initiation by slip band decohesion, especially in corrosive environments since localized strain concentrations intensify metal-environment interactions. In contrast, the nonshearable incoherent precipitates of the overaged alloy promote homogeneous deformation, leading to diffuse wavy slip bands and smaller surface offsets.[1,2]

Changes in humidity did not significantly affect the LCF resistance of the overaged alloy. These results are different from those obtained for the underaged condition in which an environmental effect was observed. The environmental sensitivity is related to the deformation mode and the homogeneity of deformation, being greatest for the case where extensive strain localization was observed. Since the strengthening precipitates are incoherent in the overaged condition, they are looped and/or bypassed by dislocations. Consequently, the deformation is relatively homogeneous and environmental sensitivity is minimal.

FATIGUE CRACK PROPAGATION BEHAVIOR

The effect of aging treatment and environment on the fatigue crack growth rates of the Al-6Zn-2Mg-0.1Zr alloy is presented in Figure 2. Growth rates of the underaged alloy tested in laboratory air, dry air and vacuum are lower than the da/dN values of the overaged alloy. The FCGR's of the underaged alloy increase in aggressive environments, especially at intermediate ranges of ΔK. Differences in crack propagation behavior for the two aging treatments can again be associated with deformation behavior.

In the underaged condition, dislocation shearing of precipitates promotes coarse planar slip and inhomogeneous deformation which favor slip plane decohesion and the occurrence of zigzag growth and crack branching. Incoherent precipitates of overaged alloys are looped by dislocations, promoting more homogeneous slip, noncrystalline fracture and a single straight running crack which lies in a plane normal to the stress axis. The FCGR has been found to decrease (for any chosen calculated ΔK) as the fracture path changes from a single straight crack to a

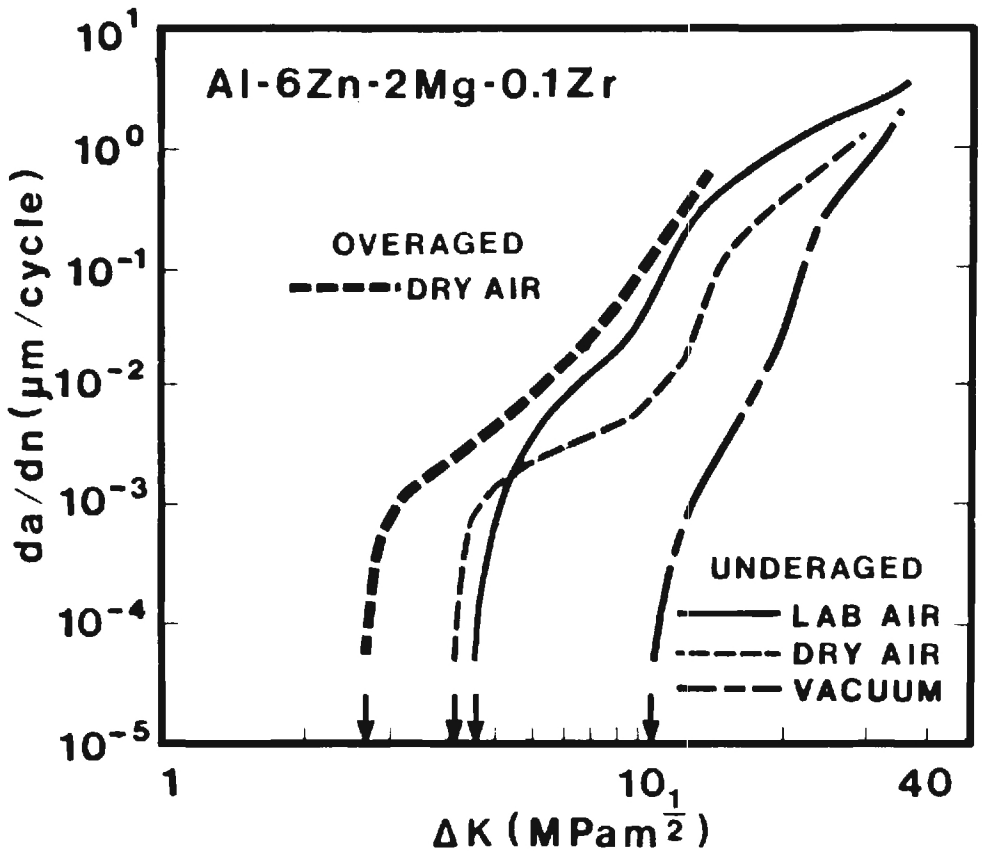

FIGURE 2. Effect of aging treatment and environment on the FCGR.

zigzag crack and then to a crack with numerous branches.[3] Planar slip and inhomogeneous deformation enhances crack branching, increases the total crack path, and lowers the effective stress intensity at the tip of the crack. This lowers the fatigue crack growth rates. The slower FCGR of the underaged alloy may also be associated with a higher degree of slip reversibility.[4]

An aggressive environment accelerates FCP over that in vacuum at equivalent values of ΔK, probably by reducing the amount of plasticity necessary for a particular increment of crack propagation.[3] It may also be due to a decrease of both slip reversibility and the rewelding process. The latter is important since a considerable difference is observed in the FCGR between dry air and vacuum, Figure 2. The environmental effect is probably associated with a form of hydrogen embrittlement in laboratory air. The exact mechanism of hydrogen embrittlement in aluminum alloys is still unknown, but it may be due to the combined action of a high pressure of hydrogen, a decrease of plasticity and a reduction of the cohesive strength of the lattice by adsorbed hydrogen. However, it is clear that the slip behavior affects the susceptibility to hydrogen embrittlement.[5,6] When strain localization occurs more hydrogen atoms can be transported by dislocations moving in the localized slip bands, thereby increasing environmental sensitivity.[3]

Eventually the FCP curves of samples tested in aggressive environments should converge to those of vacuum since at large ΔK plasticity effects dominate and occur too rapidly for chemical effects to be important. When this happens, there is a decrease in the slope of the FCP curve, as observed in Figure 2.

FRACTURE SURFACE FEATURES

SEM observations of the fracture surfaces of the underaged alloy indicate that changes of the fracture features depend not only on the test environment but also on the magnitude of ΔK. Fracture surfaces of samples tested in dry air near threshold and intermediate ranges of ΔK were crystallographic in nature

and exhibited large facets approximating the grain size. Parallel markings terminating at grain boundaries were noticed on several facets. The spacing of these markings was much too large to correspond to the crack advance per cycle. We believe these markings are due to coarse slip band offsets. It is important to note that only occasional facets showed traces of coarse slip band offsets on samples tested in vacuum at low ΔK. These results imply that slip is more reversible in the vacuum environment.

Fracture features of samples tested in laboratory air were predominately intergranular at near-threshold ΔK. Duquette[7] has proposed a hydrogen-assisted cracking model to explain the brittle type intergranular failure. Between ΔK values of 3 and 4 MPa $m^{\frac{1}{2}}$ (the "bump" region of the FCP curve) the surfaces of samples tested in laboratory air had a mixed mode of fracture. Intergranular faceting at near-threshold growth became mixed with a ductile transgranular mode as ΔK increased. At $\Delta K > 4$ MPa $m^{\frac{1}{2}}$ the laboratory air fracture surfaces were composed entirely of transgranular facets. A large proportion of these facets showed traces of coarse slip band offsets.

Frandsen and Marcus[8] have suggested that the transition from a faceted to a nonfaceted, noncrystallographic crack growth occurs when the plastic zone size exceeds the grain size. Our results indicate the disappearance of facets seems to be dependent on the FCGR instead of the relationship between the grain size and the reversed plastic zone size. For example, this transition occurs for samples tested in vacuum at ΔK = 21 MPa $m^{\frac{1}{2}}$ with the plastic zone size = 68 μm (based on plastic zone size = $0.13(\Delta K/2\sigma_y)^2$. This value exceeds the grain size, ρ = 15 μm. On the other hand, the transition in dry air is at ΔK = 14 MPa $m^{\frac{1}{2}}$ corresponding to the reversed plastic zone size = 30 μm which is much larger than the grain size. The plastic zone size for faceted to nonfaceted growth approximates the grain size only in laboratory air. The transition parameters are given in

Table I. Observations of the underaged alloy tested in the three environments consistently show the disappearance of facets occurs at da/dN = 0.1 μm. The corresponding ΔK values for samples tested in laboratory air, dry air and vacuum are 11, 14, and 21 MPa $m^{\frac{1}{2}}$, respectively. Although it is apparent that the amount of plasticity necessary for a particular increment of crack propagation decreases in aggressive environments, the mechanisms of the faceted to nonfaceted transition are not clear. This transition may be associated with the occurrence of multiple slip. Consequently, the crack growth is due to a "plastic blunting" mechanism similar to that proposed by Laird and coworkers.[9] The geometry of the plastic blunting process dictates that the fracture plane should be perpendicular to the loading direction, as observed for this region of the FCP curve. The fracture surface of samples in this region were more or less flat and composed of fatigue striations and microvoids.

TABLE I. Parameters of the Faceted to Nonfaceted Fatigue Crack Growth Transition for the Underaged Alloy

Test Environment	$\Delta K_{\frac{1}{2}}$ (MPa $m^{\frac{1}{2}}$)	Plastic Zone Size (μm)	Grain Size (μm)
Vacuum	21	68	15
Dry Air	14	30	15
Laboratory Air	11	19	15

CONCLUSIONS

(1) Strengthening precipitates of the underaged alloy are coherent and sheared by dislocations resulting in inhomogeneous deformation (strain localization.)

(2) Strain localization detrimentally affects the cyclic strain resistance. Homogenizing the deformation by overaging increases the LCF life and reduces environmental sensitivity.

(3) Strain localization affects crack propagation in two ways: it intensifies metal-environment interactions and thus accelerates crack propagation in aggressive environments; it also favors slip plane decohesion, which leads to zigzag crack growth and crack branching, both of which slow down crack propagation.

(4) The ΔK_{th} values are higher for the underaged condition than for the overaged condition, irrespective of test environment. This is probably due to a higher degree of slip reversibility and more extensive crack branching for the underaged treatment.

(5) The FCGR's are faster for the overaged condition when compared with the underaged condition at equivalent ΔK in dry air. This is related to the more homogeneous deformation and less crack branching of the overaged alloy.

(6) An aggressive environment accelerates FCP compared with the FCP in vacuum for equivalent values of ΔK, probably by a form of hydrogen embrittlement.

(7) The transition from faceted to nonfaceted noncrystallographic crack growth appears to be dependent on the FCGR instead of the relationship between the grain size and the reversed plastic zone size. The disappearance of facets may be associated with the occurrence of multiple slip. The ΔK necessary for multiple slip may decrease in the presence of an aggressive environment.

II. MODIFICATION OF THE CHAKRABORTTY MODEL FOR CALCULATING FATIGUE CRACK GROWTH RATES (Heikkenen, Chakrabortty, and Starke)

Many models[10-16] have been proposed to describe fatigue crack propagation (FCP) behavior. Most equations derived from these models are similar to that ascribed to Paris, Eq. [1], and contain adjustable constants obtainable only from FCP measurements. In addition, these equations apply only to the midrange of growth rates and provide no indication of growth rates in the near threshold regime.

$$da/dN = A(\Delta K)^n \qquad [1]$$

CHAKRABORTTY MODEL[18]

The Chakrabortty equation presented below calculates the FCGR, da/dN, using an approach suggested by Liu and Iino[19] who estimated the fatigue damage by considering the material in a volume element in the plastic zone ahead of the crack tip. As the crack propagated toward these volume elements, the cyclic plastic strain increased until crack extension occurred due to ductility exhaustion in these elements. Liu and Iino derived a FCGR expression utilizing Miner's cumulative damage law.[20] Chakrabortty has modified this approach incorporating cyclic and microstructural parameters, and the FCGR's are given by Eq. [2].

$$\frac{da}{dN} = 2\sum_n \bar{\rho}_n' \left(\Delta\varepsilon_{p_n}/2\varepsilon_f'\right)^{-1/c} \qquad \text{where } x = \frac{\Delta K^2/(1+n')\Pi E k'}{(\Delta\bar{\varepsilon}_p)^{n'+1} + \frac{k'}{E}(\Delta\bar{\varepsilon}_p)^{2n'}}$$

$$\text{and} \quad \Delta\varepsilon_{p_n} = \int_{x=r_{n-1}}^{r_n} x^{1/2}\Delta\bar{\varepsilon}_p\, dx \Big/ \int_{x=r_{n-1}}^{r_n} x^{1/2}\, dx \qquad [2]$$

The microstructural parameter, $\bar{\rho}$, is taken in terms of the mean free path between major deformation barriers and the cyclic parameters are the fatigue ductility exponent and coefficient, c and ε_f', and the cyclic strain hardening exponent and coefficient, n' and k'. The plastic strain of a volume element is represented by $\Delta\varepsilon_p$, and $\Delta\varepsilon_{p_n}$ is the constant plastic strain of the nth deformation

zone ahead of the crack tip.[18] The size of these zones is dependent on ρ'. Comparisons of predicted crack growth curves using the Chakrabortty equation with FCP data obtained experimentally show good agreement for intermediate and high values of ΔK for several alloy systems.[21,22]

At low values of ΔK (corresponding to FCGR's below $\sim 10^{-9}$m/cycle), the Chakrabortty equation overestimates the FCGR and does not accurately indicate ΔK threshold. Chakrabortty has related this overestimation at low ΔK to a grain size effect.[18] Larger grains along the crack front will experience plastic strains smaller than the strain averaged over a variety of grain sizes, $\Delta\bar{\varepsilon}_p$. As $\Delta\bar{\varepsilon}_p$ decreases with decreasing ΔK, this trend of crack retardation will continue. With increasing ΔK, this grain size effect diminishes.

The discrepancy between predicted and experimental FCGR's at low ΔK may also be related to fracture path. FCGR's are normally measured as the projected total distance of overall crack growth normal to the stress axis regardless of the crack path. The FCGR has been found to decrease with increasing crack branching. A tortuous crack path would actually be much larger than the projected crack length and can also lower the effective stress intensity at the tip of the crack, thereby lowering the measured FCGR.[3] Since crack growth values obtained by the Chakrabortty equation are based on the standard equation for ΔK for a straight crack normal to the stress axis, predicted values may overestimate measured FCGR's.[18]

CLOSURE

Experimental measurements of the FCGR have a closure component that needs to be removed before comparisons with predictive growth rates can be made. Crack closure may arise from a compressive residual stress[23] which wedge open the crack. In any event, the crack will remain closed until the applied stress overcomes the closure component. The effective applied stress intensity range, ΔK_{eff}, which actually propagates the crack is equal to the maximum applied stress intensity, K_{max} minus the value at which the crack tip just appears to open, K_{op}.[23]

Experimental FCGR's need to be plotted as a function of ΔK_{eff} for accurate comparisons with the predicted growth rates.

COMPARISON BETWEEN CALCULATED AND EXPERIMENTAL FCGR's

The results obtained by the Chakrabortty equation fall reasonably close to the expected scatter band of the experimental data at high values of ΔK for an underaged Al-6Zn-2Mg-0.1Zr alloy tested in laboratory air, Figure 3. The low cycle fatigue (LCF) and microstructural parameters used for the FCGR calculation by the Chakrabortty model are provided in Table II. The predicted FCGR was based on LCF parameters taken above the break in the Coffin-Manson plot. Our research indicates the preferred cyclic data should be selected above the break since homogeneous deformation of the microstructure at high plastic strain amplitude compares favorably with that in the plastic zone ahead of the propagating crack tip. LCF behavior below the break has been related to a strain localization phenomena.[26] Differences between the predicted and experimental crack growth curves with decreasing ΔK are believed to be created by closure and threshold effects. The experimental FCGR has been corrected for closure and the Chakrabortty equation has been modified to include a critical strain $\Delta\varepsilon_{p_{th}}$, below which fatigue damage does not occur[27] and cracks cease to propagate. These corrections are explained in the following sections and are graphically represented in Figure 4.

CLOSURE CORRECTION

The amount of fatigue crack tip closure, represented in terms of the ratio K_{op}/K_{max}, approaches 0.37 near ΔK threshold for an Al-6Zn-2Mg-0.1Zr alloy in peak-aged condition.[28] Pending further investigation of closure effects for the entire range of ΔK, these results ($K_{op}/K_{max} = 0.37$ or $\Delta K_{eff} = 0.63\ K_{max}$) will provide an approximate indication of the amount of closure.

THRESHOLD CORRECTION

The original Chakrabortty equation does not accurately indicate near threshold

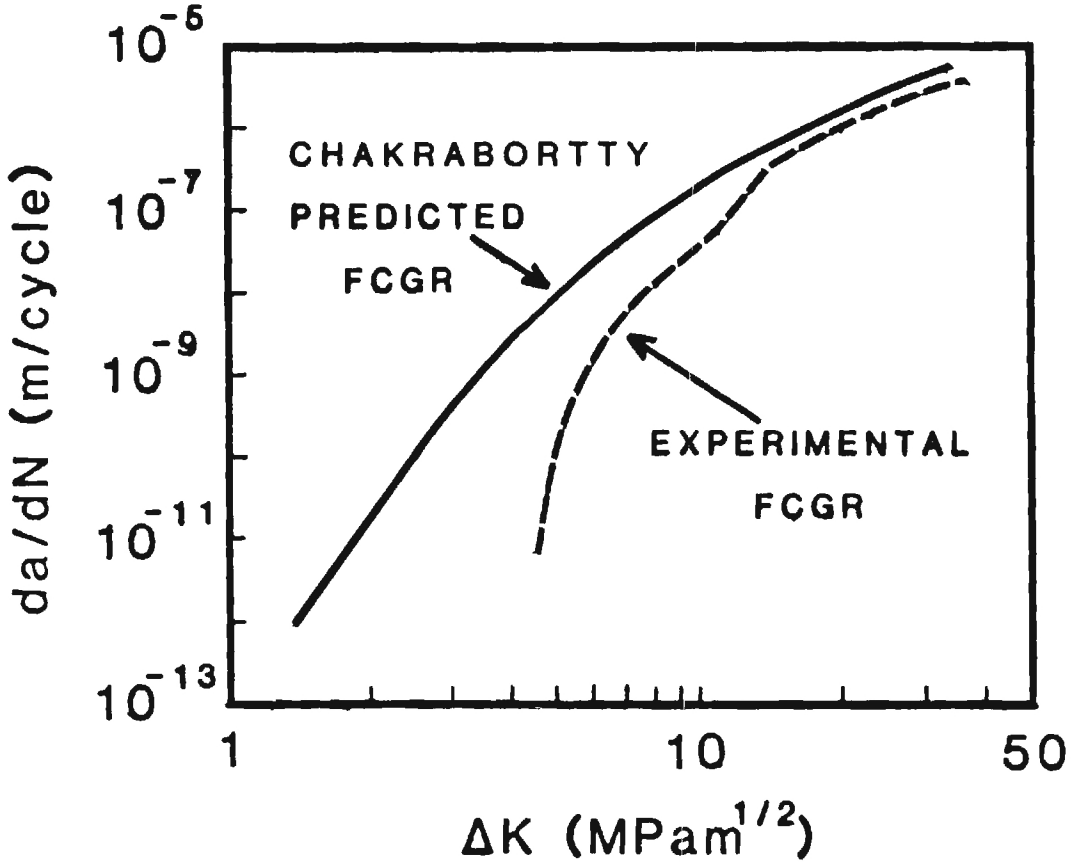

FIGURE 3. Comparison between the experimental and predicted FCGR. Alloy: Underaged Al-6Zn-2Mg-0.1Zr tested in laboratory air.

TABLE II. Cyclic and Microstructural Parameters Used for FCGR Calculation

ALLOY: Underaged Al-6Zn-2Mg-0.1Zr tested in laboratory air

c	0.562
ε_f'	0.447
n'	0.046
k'	1058 MPa
ρ'	15×10^{-6} m
E	70×10^3 MPa
$\Delta\varepsilon_{p_{th}}$	5×10^{-4}

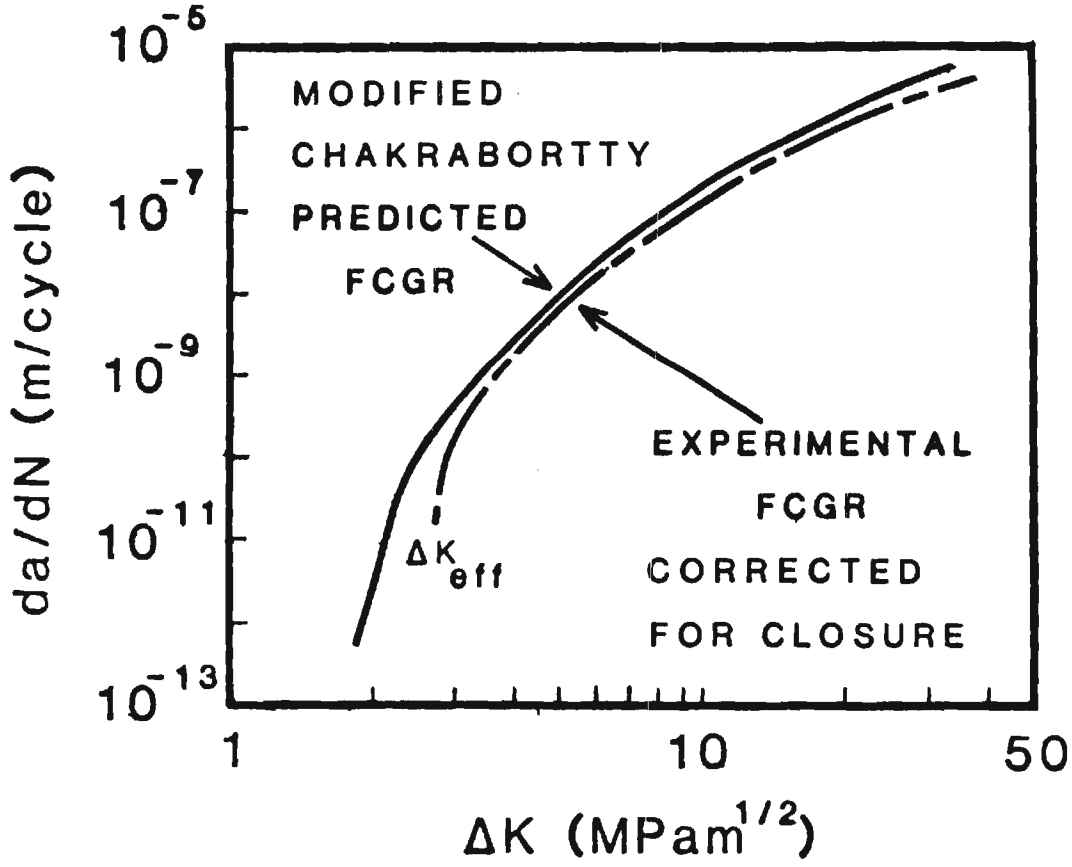

FIGURE 4. Experimental and predicted FCGR corrected for closure and threshold effects.

growth rates with decreasing ΔK. Our proposed modification is based on explaining ΔK threshold behavior in terms of a threshold plastic strain range, $\Delta\varepsilon_{p_{th}}$. This critical strain term has been incorporated directly into the Chakrabortty model in the following manner. The Coffin-Manson relation, from which the Chakrabortty model derives its cyclic parameters, was changed to accomodate the threshold plastic strain range. This new strain-life relation is expressed as:

$$\Delta\varepsilon_p/2 = \Delta\varepsilon_{p_{th}}/2 + \varepsilon_f'(2N_f)^c \qquad [3]$$

By using this correction, only the lower strain amplitude portion of the Coffin-Manson plot is changed and values of the cyclic parameters, c and ε_f', remain virtually unchanged.

$$da/dN = 2\Sigma\bar{\rho}_n[(\Delta\varepsilon_{p_n} - \Delta\varepsilon_{p_{th}})/2\varepsilon_f]^{-1/c} \qquad [4]$$

Where $\Delta\varepsilon_p$ equals the applied average strain,[18] and $\Delta\varepsilon_{p_{th}}$ is related to the onset of persistent slip band (PSB) formation.[19] Before PSB's form, slip is somewhat reversible, and cyclic plastic strain is not damaging.[18] The critical plastic strain amplitude may be determined graphically from the cyclic stress-strain (CSS) curve in a double logarithmic plot as shown in Figure 5 for a poly-crystalline material.[27] For single crystals, Regime II consists of a well-defined plateau. For our analysis, we have used a value of $\Delta\varepsilon_{p_{th}} = 5 \times 10^{-4}$ which was obtained by Lee and Laird[29] for an Al-4wt%Cu single crystal. As far as we know this is the only value available for an age-hardened aluminum alloy.

The experimentally measured value of ΔK threshold, 4.59 MPa $m^{\frac{1}{2}}$, when corrected for closure becomes 2.89 MPa $m^{\frac{1}{2}}$. The modified Chakrabortty equation predicts a threshold close to 2.00 MPa $m^{\frac{1}{2}}$. This value is certainly well within the scatter band of the experimental data and may have been closer if the grain-size-effect correction, discussed previously, could have been made.

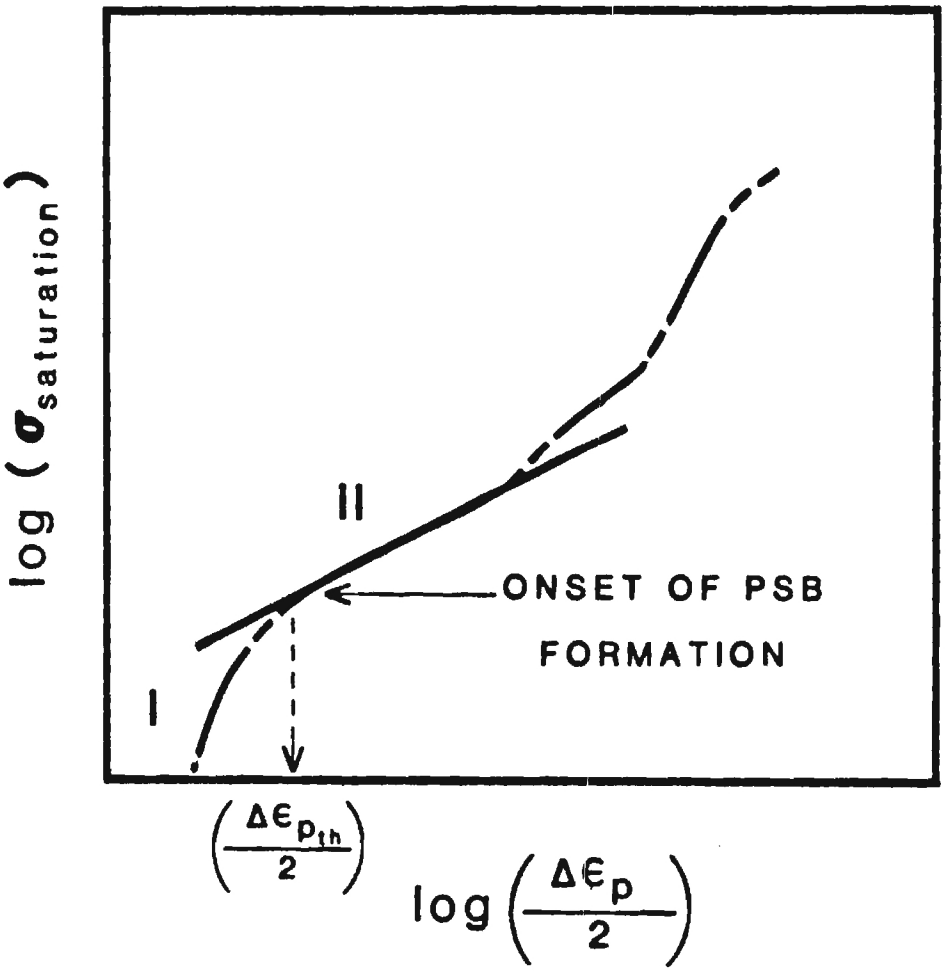

FIGURE 5. CSS curve after Mughrabi and Wang (19).

CONCLUSIONS

Comparisons between experimental and predicted FCGR's using the Chakrabortty equation showed excellent agreement at high ΔK. However, the predicted FCGR gradually begins to overestimate the measured data with decreasing ΔK. This difference is attributed to closure and threshold effects. The experimentally measured FCGR has been replotted as a function of ΔK_{eff} to account for closure, and the Chakrabortty program has been modified relating ΔK_{th} with a critical strain, $\Delta \varepsilon_{p_{th}}$, below which cracks cease to propagate. These modifications resulted in excellent agreement between the predicted and experimental crack growth curves over the entire range of ΔK.

III. THE EFFECT OF SLIP DISTRIBUTION ON THE MONOTONIC AND CYCLIC DUCTILITY OF Al-Li BINARY ALLOYS (Sanders and Starke)

There has recently been a great deal of interest in adding lithium to high strength aluminum alloys for use in aircraft components.[30,31] Each weight percent lithium added to an aluminum alloy reduces the density approximately 3% and increases the elastic modulus approximately 6%[32] for lithium additions up to 4%. However, these improvements are normally accompanied by a significant decrease in ductility.[33] The beneficial effects of lithium are realized regardless of whether or not lithium is retained in solid solution,[34] but associated slip behavior and monotonic and cyclic ductility have not always been characterized. A fundamental understanding of the influence of lithium additions on the deformation and fracture process is necessary before the maximum benefits of Al-Li-X alloys can be achieved.

Hornbogen and Zum Gahr[35] have summarized crystal-structural and microstructural features that affect slip distribution at small strains. Those that favor a heterogeneous distribution of strain, and have an adverse effect on ductility, include short range order and coherent precipitates that are sheared by dislocations. Both are present in Al-Li alloys. The Al-Li system is a simple eutectic that contains a metastable miscibility gap, Figure 6, and short range order in the solid solution.[37] Alloys of current commercial interest contain less than 3 wt.% (11.6 at.%) lithium.

When Al-Li alloys with sufficient solute are quenched from the single phase field and subsequently aged below the critical temperature that defines the metastable miscibility gap, decomposition of the supersaturated solid solution occurs by homogeneous precipitation of the ordered $L1_2$ phase Al_3Li (δ'). The similarity in structure and lattice parameter of the δ' and the fcc matrix results in a small lattice misfit (-0.18%),[38] and spherical precipitates with an interfacial energy between particle and matrix of 180 ergs/cm^2.[39] Subsequent

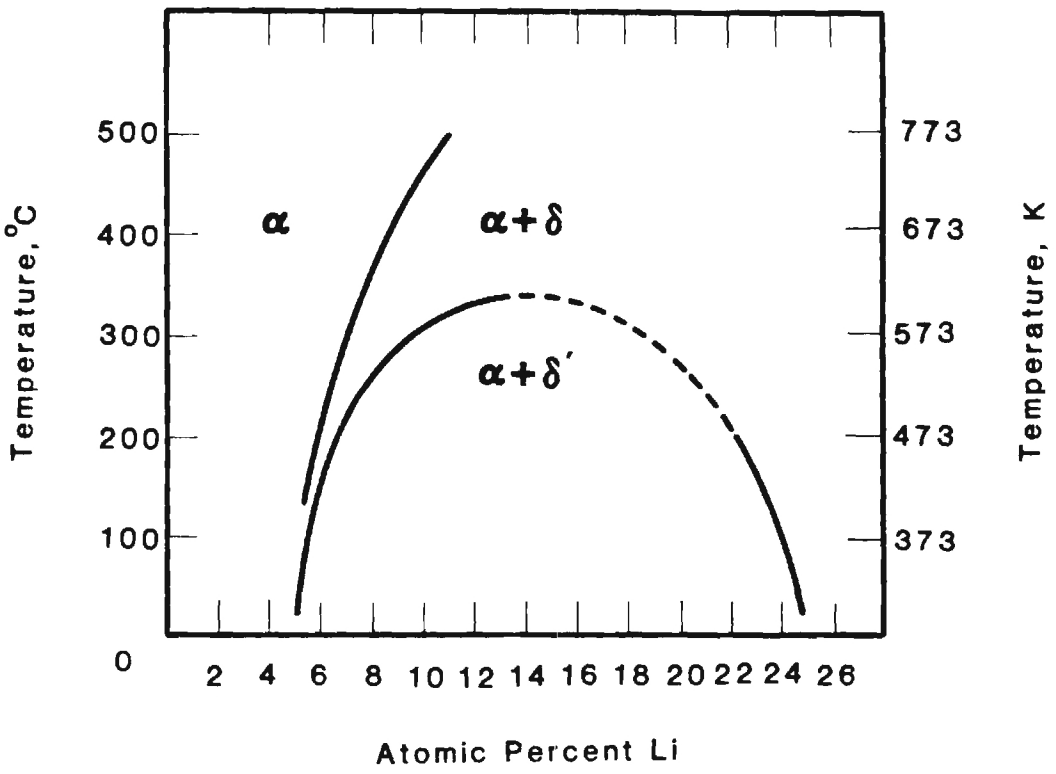

FIGURE 6. The Al-Li phase diagram showing the apparent metastable miscibility gap for δ′; after Williams. (36)

coarsening of the δ' can be described by Lifshitz-Wagner kinetics[36] with the average radius varying as $(\text{time})^{1/3}$. Concurrently, preferential precipitation and coarsening of the equilibrium AlLi (δ) phase occurs at grain boundaries, leading to the development and growth of precipitate free zones (PFZ's).[40,41]

Depending on the composition, aging time and temperature, a variety of microstructures ranging from a solid solution with short range order,[8] to two phase structures with different volume fractions and distributions of δ', δ, and PFZ's may be obtained in the Al-Li system. Short range order strengthens the alloy by increasing the frictional drag on a moving dislocation.[42] However, the passage of dislocations reduces the order across the slip plane by about 20%[43] and the second dislocation moves at a lower stress resulting in groups of dislocations and a tendency toward planar deformation at low strains.[35] The coherent precipitates also strengthen the alloy by the resistance they impart to shearing dislocations.[44] Since the interfacial energy and coherency strains between the matrix and δ' are small, the primary strengthening effect is associated with the long range order of the precipitates and is reduced when they are sheared by dislocations. This results in planar slip and a tendency toward strain localization.[35] Because of their low critical resolved shear stress, strain localization can also occur in PFZ's.[45]

The slip distribution in alloys, such as Al-Li, that contain short range order and shearable precipitates depends on the magnitude of local work softening that occurs during deformation. In many cases the work softening results in extensive strain localization and low ductility. The low ductility of Al-Li-X alloys has been associated with such phenomena.[31] Consequently, this research was directed at determining the influence of lithium content on the slip distribution and subsequent fracture behavior in simple Al-Li binary alloys. Three Al-Li binary alloys were chosen for this study: M-I: a solid solution containing

short range order (Al-3.5at.%Li); M-II: a two phase alloy having a small volume fraction of δ' (Al-5.8at.%Li); and M-III: a two phase alloy having a large volume fraction of δ' (Al-8.9at.%Li).

MICROSTRUCTURE OF UNDEFORMED SPECIMENS

The grain structures of the three alloys were identical after heat treatment and consisted of elongated recrystallized grains. No precipitates or the characteristic δ' superlattice reflections were observed during TEM examination of M-I and M-II aged for 0.25h at 473K or for M-I aged for 4h at 473K, consistent with earlier observations by Gysler, et al.[34] However, resistivity measurements[37] indicate that a binary Al-Li alloy similar to M-I should contain short range order. Selected area diffraction patterns of M-II aged for 4h at 473K contained δ' superlattice reflections, and a very fine "mottle" contrast, similar to that frequently observed during the initial stage of ordering,[46] was noted during bright field, BF, TEM examination. Superlattice reflections of δ' were present in SAD patterns of M-III in the as-quenched, AQ: AQ + 0.25h at 473K; and AQ + 4h at 473K conditions. A "mottle" contrast similar to that described for the M-II alloy was also seen in BF TEM's of AQ M-III. Well defined δ' precipitates were present for both the 0.25h and 4h conditions, and a widening of the PFZ accompanied increasing aging time, as frequently observed by other investigators.[40,41]

Because of the difficulty involved, no attempt was made to quantitatively determine the degree of short range order in M-I or the variation in size and volume fraction of δ' with concentration and aging time. However, these parameters can be estimated as follows: the maximum degree of short range order can be calculated using the Warren short range order parameter:[47]

$$\alpha_i = 1 - (Pab_i/m_b) \qquad [5]$$

where Pab_i is the probability that a b atom is in the ith shell around an a atom,

and m_b is the mole fraction of b, i.e., the random probability. For the first shell, which is the most important, the probability that the Li atom, a, is surrounded by an Al atom, b, is unity for a dilute solution like M-I. Therefore, $\alpha_1 = 1 - 1/.965 = -0.036$, a very small number. Using published information for the δ' solvus line in conjunction with our TEM results we estimate that δ' has a radius of 20Å and represents $\sim$ 2 volume percent in M-II aged 4h at 473K; a radius of 40Å and represents $\sim$ 19 volume percent in M-III aged 0.25h at 473K, and a radius of 110Å and represents $\sim$ 19 volume percent in M-III aged 4h at 473K.

Our results confirm those of other workers[36] that M-I lies outside, and M-III lies inside the metastable miscibility gap for δ' precipitation. The critical ordering temperature of Al_3Li, based on measured superlattice spacings and the associated calculated antiphase boundary energy of 195 ergs/cm^2, has been estimated to be 810K for an Al-11.7at.%Li.[39] This temperature is above the δ' solvus and essentially our quenching temperature and would suggest the presence of short range order prior to quenching. For M-III we estimate that $\alpha_1 = -0.1$, indicating extensive short range order. Considering this large value and the rapid diffusion rates of Li in Al, $D = 4.5 \exp (33{,}000/RT)$ cm^2/s,[48] and the low interfacial and misfit energy of δ', it is reasonable that homogeneous nucleation of δ' occurred during quenching of M-III, followed by simple coarsening during aging. This result is consistent with small angle x-ray diffraction[37] and TEM[38,41] coarsening kinetic studies of Al-Li alloys well within the metastable miscibility gap.

When considering the small estimated value of the short range order parameter, $\alpha_1 = 0.06$, of the more dilute M-II, and the larger diffusion distances required for Al_3Li formation it is also reasonable that its formation could be prevented during quenching. Al_3Li did form during aging at 473K and this result is in agreement with the δ' solvus line reported by Nozato and Nabai.[49]

MONOTONIC PROPERTIES AND DEFORMATION BEHAVIOR

The monotonic properties of the three alloys are summarized in Table III along with the properties of pure aluminum for comparison. Increasing the amount of lithium progressively increases the elastic modulus, yield strength, and tensile strength along with a reduction in strain to fracture. Furthermore, if the alloy contains sufficient lithium to permit precipitation, increasing the aging time results in a corresponding increase in strength and decrease in ductility. The yield strengths reported here are somewhat different from those measured by Gysler, et al[34] but the differences may be accounted for by grain size variations between the two sets of samples. In any event, the change in properties with composition was very similar. The increase in elastic modulus with lithium concentration indicates that the δ' phase is not necessary to increase the elastic modulus of Al-Li alloys. This result is consistent with the work of Gysler et al[34] and Harris and coworkers[50] and may be related to the short range order present in these alloys.

The strength increase associated with short order is proportional to the Warren short range order parameter and the atomic fraction of solute[47] and is expected to be quite small for the dilute M-I and M-II alloys which have a maximum α_1 of -0.036 and -0.06, respectively. Consequently, only a slight amount of work softening occurs due to the destruction of the short range order, and extensive strain localization does not develop as was noted in this study. On the other hand, a large degree of work softening can occur when the coherent, ordered δ' particles are sheared by dislocations. Once the particles are sheared their resistance to further dislocation motion is reduced and strain localization on the primary slip plane occurs.

The strengthening effect associated with δ' precipitates, and the associated work softening that can result when they are destroyed by intensive slip, can

TABLE III. Tensile Properties of the Al-Li Binary Alloys*

Alloy	Heat Treatment	E GPa	$\sigma_{0.2}$ MPa	σ_{uts} Mpa	ε_f %
Pure Al	Annealed	68	11.7	47	60
Al-3.5at.%Li(M-I)	811K CWQ ** + ½h @ 473K	73	22	75	43
	811K CWQ + 4h @ 473K	73	24	82	39
Al-5.8at.%Li(M-II)	811K CWQ + ½h @ 473K	76	37	96	42
	811K CWQ + 4h @ 473K	76	46	94	30
Al-8.9at.%Li(M-III)	811K CWQ + ½h @ 473K	80	137	215	21
	811K CWQ + 4h @ 473K	80	195	278	6.6

*Average of two tests
**Cold Water Quench

be estimated as follows. The motion of a unit dislocation through the ordered lattice of the δ' precipitate will not recreate the structure in its wake, but creates disorder in the form of an antiphase domain boundary. To minimize the extra energy associated with the boundary, dislocations normally move in pairs in Al-Li alloys,[41,51] similar to the superdislocations in alloys containing long range order.[52] This normally results in fine planar slip in ordered alloys, but can lead to strain localization and coarse slip after sufficient disorder has been created.[53] Using the theoretical treatment by Gleiter and Hornbogen[54,55] for misfit-free, ordered particles which are sheared by superdislocations, the increase in CRSS $\Delta\tau_o$ due to the particles is given by:

$$\Delta\tau_o = 0.28\gamma^{3/2}G^{-1/2}b^{-2}f^{1/2}r_o^{1/2} \qquad [6]$$

where γ is the antiphase boundary energy, f the volume fraction of particles G the shear modulus of the matrix, b the Burgers vector and r_o the mean particle radius. Figure 7 shows a plot of the measured yield strength versus $r_o^{1/2} f^{1/2}$. It is interesting to note that, not only does the data for M-II and M-III lie on a straight line, but the line intersects the ordinate at the yield stress for M-I which contains no δ' precipitates. Since all terms in Eq. [6] but $r_o^{1/2} f^{1/2}$ are the same for each alloy and heat treatment, the magnitude of this product should be proportional to the degree of work softening possible during deformation, and thus describe the tendency toward localized slip. Figure 7 suggests that M-II should deform homogeneously and similar to M-I but that M-III should deform heterogeneously in both aged conditions.

The observed decrease in macroscopic ductility with increasing lithium content and aging time can be explained qualitatively by the corresponding increased tendency for planarity and inhomogeneity of slip. As deformation becomes more concentrated in narrow slip bands, crack nucleation can occur at lower macroscopic strains.

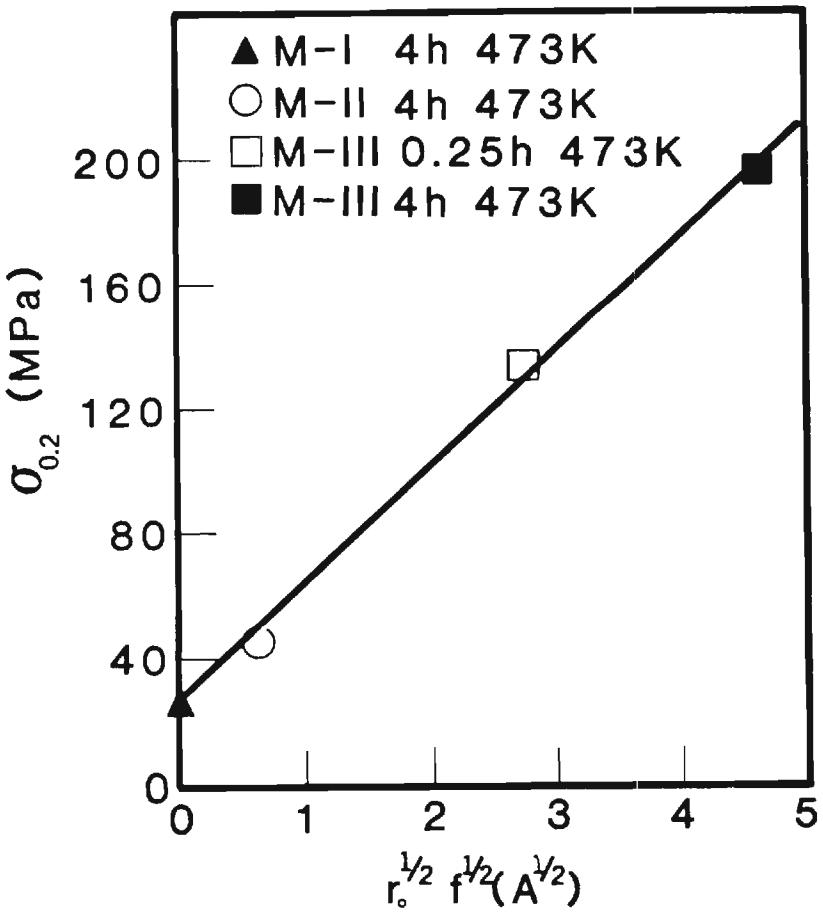

FIGURE 7. Yield stress plated as a function of the product of the size and volume fraction of δ'.

STRAIN-LIFE, DEFORMATION, AND FRACTURE OF FATIGUE SAMPLES

Since fatigue damage is caused by cyclic plastic strain, the fatigue life may be related to this parameter.[1] The plastic strain amplitude, $\Delta\varepsilon_p/2$, versus the reversals to failure, $2N_f$ (Coffin-Manson plots) of M-II and M-III aged for 4h at 473K, show that the low cycle fatigue life for M-II is considerably longer than that of M-III at an equivalent strain amplitude, Figure 8. Although such plots include both reversals to initiation and reversals connected with crack propagation, most of the life is spent in the initiation stage and similar differences would appear if the abscissa were reversals to initiation. Such plots are usually not made because of the uncertainty involved in determining the cycles at which the fatal crack is created. Analysis of the hystereses loops associated with the data presented in Figure 8 indicated that the differences in fatigue life between M-II and M-III is primarily due to differences in fatigue crack initiation resistance. The higher degree of local cyclic softening due to the larger volume fraction of shearable δ' precipitates in M-III, enhances strain localization. This results successively in an increased dislocation density on the glide plane, large slip offsets on the surface, concentration of stress, and early fatigue crack initiation.[1]

Once the fatal crack was formed in M-II, crack propagation occurred for all strain amplitudes by the noncrystallographic, striated growth mechanism associated with plastic blunting by Laird and coworkers.[56] However, crack propagation proceeded primarily along slip planes for M-III, although the "link-up" of cracks and final fracture due to overload was intergranular. Koss and Chan[57] have theoretically examined the conditions for fracture along a planar slip band. They concluded from their analysis that once a crack nucleates along an intense slip band, activation of secondary slip is difficult. This results in large hydrostatic and normal stresses near the crack tip and easy crack propagation. Their treatment explains the differences in

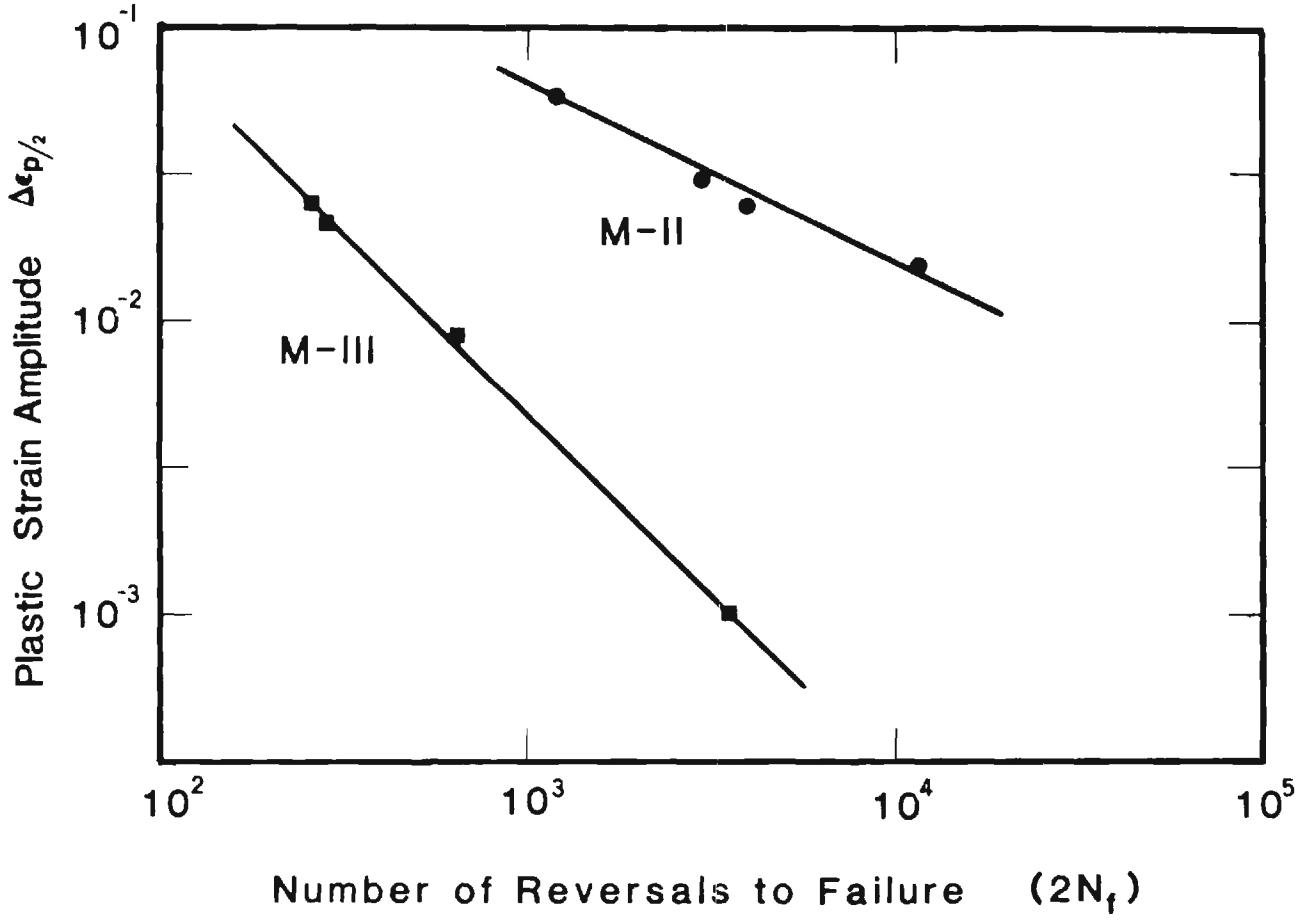

FIGURE 8. Strain life curves for M-II and M-III aged 4h at 473K.

crack propagation mode associated with the variance in strain localization of M-II and M-III.

CONCLUSIONS

Our study has shown that Al-5.8at.%Li lies just inside the metastable miscibility gap for δ' precipitation, and Al-8.9at.%Li lies well within the two phase field making the alloy responsive to age hardening. The observed deformation behavior was related to the different microstructures and controlled both monotonic and cyclic ductility. The usual gradual loss in ductility accompanied the strength improvement due to increased alloy concentration, but incipient brittleness linked with grain boundary fracture, occurred for the M-III alloy aged 4h at 473K. This grain boundary fracture is not likely due to segregation of tramp elements, as previously thought, but due to strain localization associated with a large volume fraction of shearable δ' precipitates. Concentrated slip shears the grain boundaries producing offsets which act as crack nuclei at small strains. These cracks concentrate the stress, and plastic flow and subsequent crack extension follows the soft PFZ's along grain boundaries resulting in a low macroscopic strain to fracture. Strain localization also reduces the fatigue crack initiation resistance and enhances fatigue crack propagation along intense slip bands.

The detrimental effect of lithium is associated with the presence of the ordered δ' precipitates. Small lithium additions, which go into solid solution or only slightly exceed the solubility limits for δ' formation, have no adverse effect and are very beneficial since they increase the elastic modulus and lower the density of aluminum. Based on these observations, one possible way of utilizing the beneficial aspects of lithium is to add up to 5.8 at.% Li to dispersion hardened aluminum alloys.

IV. MICROSTRUCTURE-PROPERTY RELATIONSHIPS OF TWO Al-3Li-2Cu-0.2Zr-XCd ALLOYS (Lin, Chakrabortty, and Starke)

Earlier work showed that additions of copper, together with small additions of cadmium, considerably increase the strength of Al-Li alloys with no corresponding decrease in ductility.[58] Cadmium has been shown to facilitate the precipitation of θ' in Al-Cu alloys[59-62] and was probably added in the old commercial 2020 (Al-4.45Cu-1.2Li-0.5Mn-0.2Cd) alloy for that purpose. Cadmium may also aid in the formation of the T_1 (Al_2CuLi) and T_2 (Al_6CuLi_3) phases in Al-Li-Cu alloys.[59] Our work[63,64] has shown that the degree of recrystallization and the recrystallized grain size of 2020-T651 plate is larger than that observed in other 2XXX alloys having no cadmium, indicating that cadmium may enhance recrystallization. Zirconium, which precipitates as coherent Al_3Zr in many aluminum alloys, has been shown to inhibit recrystallization and grain growth during solutionizing treatments.[65] The purpose of this investigation was to examine the effect of cadmium on the recrystallization, precipitation and tensile fracture behavior of an Al-3wt.%Li-2wt.%Cu-0.2wt.%Zr alloy. The nominal compositions selected for this study were Al-3wt.%Li-2wt.%Cu-0.2wt.%Zr and Al-3wt.%Li-2wt.%Cu-0.2wt.%Zr-0.2wt.%Cd.

EFFECT OF Cd ON THE RECRYSTALLIZATION BEHAVIOR

The degree of recrystallization (DR) was determined after the various solutionizing treatments for both alloys. The Cd-free alloy did not recrystallize regardless of the solutionizing temperature. The unrecrystallized structure was very uniform, and the unrecrystallized grains were composed of fine subgrains. TEM studies showed that the subgrain diameter varied from 1 to 10 μm. The 0.2% Cd alloy recrystallized either partially or totally, depending on the solutionizing temperature. For treatments below 763K the alloy remained unrecrystallized. However, after solutionizing at 798K the structure consisted

of large unrecrystallized regions and large recrystallized regions. After solutionizing at 811K the unrecrystallized and recrystallized regions were intermixed on a finer scale, and after solutionizing at 823K, the structure was almost completely recrystallized. An unrecrystallized microstructure, similar to that obtained in the Cd-free alloy, was obtained in the Cd-containing alloy by preheating at 763K prior to solutionizing at higher temperatures.

X-ray diffraction analysis indicated that both alloys contained the same type of precipitates in the as-extruded condition and after the various solutionizing treatments, Table IV. However, orientation effects prevented a determination of the volume fraction of the various phases detected in the x-ray patterns. In the as-extruded condition the equilibrium phases T_2 and δ and the constituent phase Al_7Cu_2Fe were present. The δ lines were very weak after solutionizing at 763K, they disappeared after the 813K treatment, and reappeared after aging for 16h at 473K. Diffraction lines from the δ' and T_1 phases were detected after aging.

In the as-extruded condition, both alloys had a well defined subgrain structure with 0.5 to 1 μm precipitates along the subgrain boundaries. These precipitates were identified by selected area diffraction (SAD) analyses as the equilibrium phases T_2 and δ. Scanning electron microscopy of bromine-etched samples showed that numerous large particles ($\sim$5-10 μm) were present both before and after solutionizing. This fact, taken in conjunction with the reduction in diffraction intensity, indicates that most of the small particles observed by SEM were δ. Although no quantitative measurements were made, it was obvious from the examination of many samples that there were more of the large particles in the Cd-containing alloy. The results of EDXA on the coarse precipitates after various heat treatments are given in Table V. X-ray intensities emitted from a specimen under the electron beam are not, in general, linearly propor-

TABLE IV. Precipitates Detected in Guinier-Patterns of the Al-3Li-2Cu-0.2Zr-0.XCd Alloys

PHASE	AS EXTRUDED	SHT 763K CWQ*	SHT 763K +813K CWQ	SHT 813K CWQ	SHT 813K CWQ + AGE
T_2	D-M	D-M	D-M	D-M	D-M
δ	D-S	D-VW	---	---	D-VW
δ'	---	---	---	---	D-S
T_1	---	---	---	---	D-W
Al_7Cu_2Fe	D-VW	D-VW	D-VW	D-VW	D-VW

D-VW: Detected-Very Weak
D-W : Detected-Weak
D-M : Detected-Medium
D-S : Detected-Strong
*CWQ: Cold Water Quenched

TABLE V. Energy Dispersive X-ray Analysis: Ratio of Intensity in Matrix (M) and Large Particles (P) to a Pure Standard

As-Extruded - Cd-Free

Element	M	P-1	P-2	P-3	P-4
Cu	0.008	0.13	0.12	0.08	0.11
Fe	0.003	0.04	0.06	0.06	0.09
Zr	0.004	0.006	0.008	0.008	0.005
Cd	0.001	0.001	0.001	0.001	0.001
Al	0.95	0.41	0.41	0.37	0.31
Al/Cu	-----	3.2/1	3.4/1	4.6/1	2.8/1
Corrected Al/Cu		5/1	5/1	7/1	4/1

As-Extruded - 0.2% Cd

Element	M	P-1	P-2	P-3	P-4
Cu	0.007	0.11	0.12	0.12	0.11
Fe	0.002	0.009	0.007	0.007	0.006
Zr	0.004	0.005	0.005	0.005	0.006
Cd	0.012	0.023	0.023	0.023	0.023
Al	0.96	0.43	0.44	0.44	0.44
Al/Cu	-----	3.9/1	3.7/1	3.7/1	4/1
Corrected Al/Cu		6/1	5/1	5/1	5/1

0.2% Cd Annealed 763K CWQ

Element	M	P-1	P-2	P-3	P-4	P-5
Cu	0.017	0.17	0.16	0.18	0.12	0.15
Fe	0.002	0.003	0.003	0.004	0.007	0.006
Zr	0.005	0.008	0.008	0.008	0.007	0.007
Cd	0.015	0.026	0.028	0.028	0.025	0.023
Al	0.96	0.73	0.62	0.62	0.61	0.62
Al/Cu	-----	4.3/1	3.9/1	3.4/1	5/1	4.1/1
Corrected Al/Cu		6/1	6/1	5/1	7/1	6/1

Cd-Free - Annealed 813K CWQ

Element	M	P-1	P-2	P-3	P-4	P-5
Cu	0.024	0.11	0.27	0.17	0.12	0.16
Fe	0.005	0.04	0.008	0.006	0.016	0.012
Zr	0.005	0.008	0.006	0.006	0.006	0.008
Cd	0.001	0.001	0.001	0.001	0.001	0.001
Al	0.96	0.60	0.41	0.27	0.68	0.62
Al/Cu	-----	5.5/1	1.5/1	1.6/1	5.7/a	3.9/1
Corrected Al/Cu		8/1	2/1	2/1	8/1	6/1

0.2% Cd Annealed 813K CWQ

Element	M	P-1	P-2	P-3	P-4	P-5
Cu	0.018	0.14	0.09	0.15	0.12	0.16
Fe	0.002	0.017	0.12	0.09	0.11	0.06
Zr	0.005	0.011	0.010	0.011	0.012	0.010
Cd	0.014	0.039	0.048	0.039	0.037	0.040
Al	0.95	0.79	0.27	0.75	0.72	0.62
Al/Cu	-----	5.6/1	3/1	5/1	6/1	3.9/1
Corrected Al/Cu		8/1	4/1	7/1	9/1	6/1

tional to the chemical composition. Conversion of x-ray data to composition requires correction for instrument errors, background, and physical interactions in the sample. The major corrections include mass absorption, fluorescence, and that due to the emergence angle. The aluminum is attenuated by approximately 47% more than copper for the conditions of our measurements. The corrected Al/Cu ratios listed in Table V, taken in conjunction with the x-ray diffraction results, indicate that most of the large particles are the T_2 phase and the others are Al_7Cu_2Fe. Transmission electron microscopy studies showed that, in the as-extruded condition, a high dislocation density was associated with the large particles.

The large T_2 and Al_7Cu_2Fe particles, and associated deformation structure, may act as nucleating sites for recrystallization,[66-69] and thus influence the recrystallization behavior. However, with the exception of some minor differences, this structure was present in both alloys and it is unlikely that the large difference observed in the recrystallization behavior can be due solely to such a small microstructural difference. Therefore, other factors which might influence the recrystallization behavior have to be considered.

The as-solutionized microstructure of the Cd-free alloy, and the Cd-containing alloy given the preheat, were essentially identical. Both contained a well defined subgrain structure, a much smaller volume fraction of the 0.5-1 μm T_2 and δ phase particles than observed in the as-extruded condition, and Al_3Zr precipitates. Al_3Zr and Al_3Li have the same crystal structure and lattice parameter and are difficult to separate in TEM's of aged alloys. However, the δ′ solvus temperature of an Al-3Li alloy is approximately 573K, and although δ′ may form during quenching from above the solvus temperature, it is unresolvable in BF TEM's.[33] Al_3Zr is stable at the solutionizing temperature and is present in solutionized and quenched samples. These small coherent precipitates are very

effective in inhibiting recrystallization and grain growth. Rystad and Ryum[65] have suggested that the coherent nature of their interface imparts a high drag force on the recrystallization front since the precipitate matrix interface has to change from coherent to semicoherent or incoherent as the recrystallization front passes the Al_3Zr precipitate. During solutionizing both alloys have large particles which enhance recrystallization, and small Al_3Zr particles which inhibit recrystallization. The stability of a deformed aluminum alloy having a bimodal particle distribution has been analyzed by Nes[70] who showed that a suitable distribution of fine particles could prevent growth of nuclei formed at large particles.

Energy dispersive x-ray analysis indicated that some zirconium was associated with the large T_2 and Al_2CuFe particles, Table V. The zirconium concentration in the particles was statistically higher in the Cd-containing alloy solutionized in 813K than in the Cd-free alloy given the same treatment. When the Cd-containing alloy was given the preheat at 763K, a lower concentration of zirconium, similar to that obtained for the Cd-free alloy, was observed in the large particles. It appears that in the presence of cadmium, zirconium either enters into, or precipitates on, the coarse Al_7Cu_2Fe and T_2 particles during high temperature annealing. This does not occur during annealing at 763K. The influence that cadmium has on the recrystallization behavior of the Al-3Li-2Cu-0.2Zr alloy may simply be due to its tying up more of the zirconium in the T_2 and Al_7Cu_2Fe phases and thus reducing the volume fraction of Al_3Zr. During the low temperature preheat most of the zirconium precipitates as Al_3Zr and recrystallization is suppressed during subsequent high temperature treatments. Although this interpretation may explain the present results, it does not explain why cadmium appears to enhance recrystallization in Zr-free alloys such as 2020. It is possible that the role of cadmium in nucleating large second phase particles

may have a significant effect on recrystallization in these cases. Obviously, a more extensive study of this phenomenon would be of interest.

The effect of the solutionizing temperature on the hardness of the aged alloys is shown in Figure 9. The Cd-free alloy shows an increase in hardness as the solutionizing temperature is increased up to 813K. The variance in the five hardness readings used to determine the average values plotted in Figure 9 was ± 3%. The higher solutionizing temperature increases the solid solubility (reducing the amount of primary T_2 phase) which increases the amount of solute that can form strengthening precipitates during subsequent aging. A similar hardness behavior is also observed for the Cd-containing alloy when the alloy is given the preheat treatment discussed earlier. However, when solutionized without the preheat treatment, the hardness data appeared erratic, Figure 9, with a deviation from the average of ± 13%. This behavior can be explained in terms of the mixed grain structure of the material. When the hardness measurement was made on the recrystallized area a low hardness value was obtained because of the loss of substructure strengthening in these regions.

EFFECT OF CADMIUM AND STRETCHING ON THE AGING BEHAVIOR

For a given solutionizing and aging treatment, and identical grain structure, the hardness values of the Cd-free alloy always appear higher than those for the Cd-containing alloy, Figure 9. The apparent reason for this behavior is that the presence of cadmium tends to stabilize the large T_2 precipitates thus removing some of the copper and lithium from forming the T_1 and δ' strengthening precipitates during aging.

TEM studies were conducted in order to determine the effect of cadmium and stretching on the precipitation behavior of the two alloys with a similar, unrecrystallized, grain structure. The results can be summarized as follows: In the unstretched and aged condition, the Cd-containing alloy had more subgrain

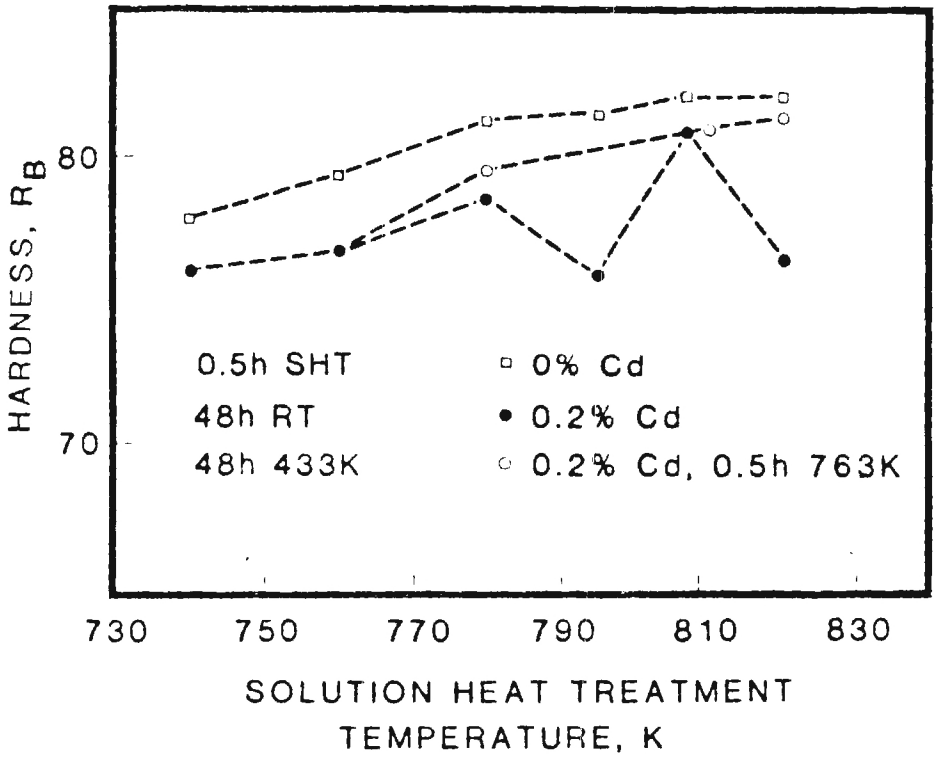

Figure 9. The effect of the SHT on the hardness of aged Al-3Li-2Cu-0.2Zr alloys with and without 0.2%Cd.

and grain boundary precipitates. Stretching prior to aging reduced the amount of subgrain and grain boundary precipitates which were identified as T_2 and δ from SAD analyses. They appear to nucleate at the grain boundary and grow only into one grain, even though tilting experiments showed that the δ' precipitate free zone was present on both sides of the grain boundary.

Both δ' and T_1 matrix precipitates were identified by TEM and SAD analysis. The platelet (or lath) -type T_1 precipitates have the {111} habit plane observed by other researchers.[38] In the unstretched condition, the T_1 precipitates were observed either on low angle (subgrain) boundaries or in isolated areas within the grains (most likely on dislocations). The Cd-containing alloy did not appear to have more T_1 than the Cd-free alloy. Al_3Li precipitate free zones were not observed around some of the subgrain boundaries that were free of the large precipitates.

Stretching prior to aging seems to reduce the amount of subgrain boundary precipitation for both alloys. However, no significant change in the δ' PFZ was observed. Stretching greatly increases the amount of T_1 precipitation within the matrix. The PFZ for T_1 appears to be smaller than that for δ'. In fact, the T_1 lath spacing appears to be as large or larger than the distance between the grain boundaries and the nearest T_1 precipitates. Cadmium does not appear to significantly influence the precipitation behavior of the stretched alloys.

TENSILE PROPERTIES

The tensile properties for the two alloys in the unrecrystallized condition are given in Table VI. The Cd-containing alloy has a slightly higher yield strength in the as-quenched condition; however, the yield strength is either equal to or slightly lower than the Cd-free alloy for aging times up to and including 16h at 463K. The yield strength is somewhat lower in the overaged condition (by 46 MPa) and the stretched and 16h aged condition (by 30 MPa).

TABLE VI. Tensile Properties

Aging	Cd-free - Unrecrystallized			0.2%Cd - Unrecrystallized		
	σ_{02} MPa (ksi)	σ_{uts} MPa (ksi)	ε_f %	σ_{02} MPa (ksi)	σ_{uts} MPa (ksi)	ε_f %
As Quenched	179 (26)	392 (57)	15.2	192 (28)	384 (56)	16.2
3h @ 463K	424 (62)	528 (77)	5.2	422 (62)	510 (74)	4.3
10h @ 463K	472 (69)	558 (81)	3.6	447 (65)	528 (77)	3.6
16h @ 463K	445 (65)	552 (81)	5.7	441 (64)	556 (81)	5.5
48h @ 463K	440 (64)	538 (79)	5.8	394 (58)	496 (72)	5.6
2% Stretch + 16h @ 463K	503 (73)	561 (82)	4.0	473 (69)	550 (80)	4.2

Since cadmium atoms have a high binding energy with vacancies,[71] they may act as a vacancy pump[72,73] in the late stages and thus accelerate the overaging effects. The presence of cadmium does not seem to induce the same positive effect on precipitation of these high Li:Cu ratio alloys as it does on low Li:Cu ratio alloys. This confirms the earlier suggestion by Silcock[59] that cadmium has a significant effect on the nucleation of θ' but only a minor effect on the nucleation of T_1.

The elongation to fracture dropped off sharply with the initial aging step and remained relatively constant as aging progressed. Neither the presence of cadmium nor the stretching treatment significantly affect the ductility; however, the highest strength was obtained for the stretched and aged alloys. The effect of degree of recrystallization on the tensile properties is shown in Table VII. The yield strength decreases with DR; probably due to a loss in substructure strengthening. There appears to be a small increase in elongation with increase in DR.

TABLE VII. Effect of DR on the Tensile Properties of Al-3Li-2Cu-0.2Zr-0.2Cd

Degree of Recrystallization (%) in Gage Section	$\sigma_{0.2}$ MPa (ksi) aged 16h @ 463K	σ_{uts} MPa (ksi)	ε_f (%)
0	441 (64)	556 (81)	5.5
27	416 (61)	524 (77)	5.5
60	373 (54)	493 (72)	6.9
60*	426 (62)	517 (75)	7.0

*Given 2% stretch prior to aging.

CONCLUSIONS

(1) Cadmium has a significant effect on the recrystallization behavior of Al-Li-Cu-Zr alloys. It appears to tie up some of the zirconium during high temperature annealing and thus reduce the volume fraction of the recrystallization-inhibiting precipitate Al_3Zr.

(2) Cadmium does not aid in the precipitation of the strengthening precipitates T_1 and δ' in the Al-3Li-2Cu-0.2Zr alloy. It has a detrimental effect since it increases the formation of the coarse equilibrium grain boundary precipitates. This reduces the amount of lithium and copper available to form the strengthening precipitates.

(3) A stretch prior to natural and artificial aging increases the strength with no significant loss in ductility. The dislocations generated by the stretch act as nucleating sites for the T_1 precipitates.

(4) The low ductility observed for these alloys in the aged conditions is most likely associated with strain localization either in coarse slip bands or in PFZ's.

PROFESSIONAL PERSONNEL

Dr. Edgar A. Starke, Jr.
Dr. Thomas H. Sanders, Jr.
Dr. Saghana B. Chakrabortty
Dr. Fu-Shiong Lin
Dr. M. Marek

GRADUATE STUDENTS

Charles Heikkenen
Paul Niskanen
John Rinker

DEGREES GRANTED UNDER AFOSR-78-3471

Fu-Shiong Lin, "Low Cycle Corrosion Fatigue and Crack Propagation of High Strength 7XXX-Type Aluminum Alloys," Doctor of Philosophy, April, 1978.

Bhaskar Sarkar, "Stress Corrosion Characteristics of Al-Zn-Mg Alloys with Copper Additions," Doctor of Philosophy, August, 1979.

Herman Charles Heikkenen, "A Study of the Fatigue Behavior of an Al-6Zn-2Mg-0.1Zr Alloy," Master of Science in Metallurgy, November 1981.

PUBLICATIONS UNDER AFOSR-78-3471

Fu-Shiong Lin and E. A. Starke, Jr., "The Effect of Copper Content and Degree of Recrystallization on the Fatigue Resistance of 7XXX-Type Aluminum Alloys, I. Low Cycle Corrosion Fatigue," Mater. Sci. and Engr., 39, 27-41 (1979).

E. E. Underwood and E. A. Starke, Jr., "Quantitative Stereological Methods for Analyzing Important Microstructural Features in Fatigue of Metals and Alloys," in STP 675, ASTM, Philadelphia, PA, 633-682 (1979).

Fu-Shiong Lin and E. A. Starke, Jr., "The Effect of Copper Content and Degree of Recrystallization on the Fatigue Resistance of 7XXX-Type Aluminum Alloys, II. Fatigue Crack Propagation," Mater. Sci. and Engr., 43, No. 1, 65-76 (1980).

Fu-Shiong Lin and E. A. Starke, Jr., "The Effect of Copper Content and Deformation Mode on the Corrosion Fatigue Crack Growth Behavior of Al-6Zn-2Mg-XCu Alloys at Low Stress Intensities," Mater. Sci. and Engr., 45, 153-165 (1980).

E. A. Starke, Jr. and Fu-Shiong Lin, "Microstructure-Environment Influence on the Fatigue Behavior of Aerospace 7XXX Aluminum Alloys," Proceedings Institute of Environmental Sciences, 131-135, Philadelphia, PA (1980).

Fu-Shiong Lin and E. A. Starke, Jr., "Mechanisms of Corrosion Fatigue Crack Propagation of 7XXX Aluminum Alloys in Aqueous Environments," in Hydrogen Effects in Metals, ed. I. M. Bernstein and Anthony W. Thompson, TMS-AIME, 485-492 (1980).

B. Sarkar, M. Marek, and E. A. Starke, Jr., "The Effect of Copper Content and Heat Treatment on the SCC Behavior of Al-6Zn-2Mg-XCU Alloys," Met. Trans. A, 12A, 1939-1943 (1981).

P. Niskanen, T. H. Sanders, Jr., M. Marek, and J. G. Rinker, "The Influence of Microstructure on the Corrosion of Al-Li-Al-Li-Mn, Al-Li-Mg, and Al-Li-Cu Alloys in 3.5% NaCl Solution," in Aluminum-Lithium Alloys, ed. T. H. Sanders, Jr. and E. A. Starke, Jr., TMS-AIME, 347-376 (1981).

E. A. Starke, Jr., T. H. Sanders, Jr., and I. G. Palmer, "New Approaches to Alloy Development in the Al-Li System," J. of Metals 33, 24-33 (1981).

H. C. Heikkenen, Fu-Shiong Lin and E. A. Starke, Jr., "The Low Cycle Fatigue Behavior of High Strength 7XXX-Type Aluminum Alloys in the T7351 Condition," Mater. Sci. and Engr. 51, 17-23 (1981).

F. S. Lin, S. B. Chakrabortty and E. A. Starke, Jr., "Microstructure-Property Relationships of Two Al-3Li-2Cu-0.2Zr-XCd Alloys," Met. Trans. A. 13A, (1982).

H. C. Heikkenen, F. S. Lin and E. A. Starke, Jr., "The Relationship Between Microstructure, Cyclic-Stress Strain Response and Fatigue Crack Propagation in Al-Zn-Mg Alloys," Aluminium (in press).

T. H. Sanders, Jr. and P. W. Niskanen, "Microstructure, Mechanical Properties and Corrosion Resistance of Al-Li-X Alloys - An Overview," Res Mechanica Letters 1, 363-370 (1981).

P. Niskanen, T. H. Sanders, Jr., J. G. Rinker and M. Marek, "Corrosion of Aluminum Alloys Containing Lithium", Corrosion Science (in press).

Edgar A. Starke, Jr., "Aluminum Lithium Alloys," in 1981 Year Book of Science and Technology, McGraw-Hill Company, New York (in press).

H. C. Heikkenen, F. S. Lin, and E. A. Starke, Jr., "The Effect of Environment on the Low Cycle Fatigue Life and Fatigue Crack Propagation Behavior of an Al-6Zn-2Mg-0.1Zr Alloy," in Environmental Degradation of Engineering Materials, ed. M. R. Louthan, Jr., R. P. McNitt and R. D. Sesson, Jr., VPI, Blacksburg, VA, 459-469 (1981).

T. H. Sanders, Jr., and E. A. Starke, Jr., "The Effect of Slip Distribution on the Monotonic and Cyclic Ductility of Al-Li Binary Alloys," Acta Met. (in press).

H. C. Heikkenen, E. A. Starke, Jr. and S. B. Chakrabortty, "Modification of the Chakrabortty Model for Calculating Fatigue Crack Growth Rates," submitted to Scripta Met.

REFERENCES

1. E. A. Starke, Jr. and G. Lütjering, in Fatigue and Microstructure, ASM, Metals Park, OH, 205-243 (1979).

2. E. A. Starke, Jr. and F. S. Lin, in Proceedings of the Institute of Environmental Sciences, Vol. 5, 131-135 (1980).

3. F. S. Lin and E. A. Starke, Jr., Mater. Sci and Engr., Vol. 43, 65-76 (1980).

4. J. Lindigkeit, G. Terlinde, A. Gysler and G. Lütjering, Acta Met., Vol. 27, 1717 (1979).

5. M. R. Louthan, Jr., F. R. Caskey, Jr., J. A. Donavan and R. E. Rawl, Jr., Mater. Sci. and Engr., Vol. 10, 357 (1972).

6. M. R. Louthan, Jr., Hydrogen in Metals, ASM, Metals Park, OH, 53, (1974).

7. D. J. Duquette, Mechanisms of Corrosion Fatigue of Aluminum Alloys, Technical Report to the Office of Naval Research (1981).

8. J. D. Frandsen and H. L. Marcus, Scripta Met., Vol. 9, 1089 (1975).

9. C. Laird and R. de la Veux, Met. Trans. A, Vol. 8, 657 (1977).

10. W. Weibull, Acta Met., 11, 725 (1963).

11. F. A. McClintock, in Fracture of Solids, Drucker and Gilman, eds., Inter-Science Publishers, NY, 65.

12. H. W. Liu, Appl. Mater. Res., 3, 229 (1964).

13. A. J. McEvily and T. L. Johnston, Int. J. Frac. Mech., 3, 45 (1967).

14. J. R. Rice, in Fatigue Crack Propagation, ASTM STP 415, 247 (1967).

15. J. Weertman, Int. J. Fract., 9, 125 (1973).

16. S. D. Antolovich, A. Saxena and G. R. Chanani, Eng. Fract. Mech., 7, 649 (1975).

17. P. C. Paris and F. Erdogan, Trans. ASME, J. Basic Eng., 85D, 528, (1963).

18. S. B. Chakrabortty, Fat. Eng. Mater. and Structures, 2, 331 (1979).

19. H. W. Liu and N. Iino, Proc. 2nd Intl. Conf. on Fract., 812 (1969).

20. M. S. Miner, J. Appl. Mech., 12A, 159 (1945).

21. S. B. Chakrabortty and E. A. Starke, Jr., Met. Trans., 10A, 1981 (1970).

22. E. J. Coyne, Jr. and E. A. Starke, Jr., Int. J. Fract., 15, 405 (1979).

23. W. Elber, Eng. Fract. Mech., 2, 37 (1970).

24. S. Suresh, G. F. Zamiski and R. O. Ritchie, Met. Trans., 12A, 1435 (1981).

25. K. Minakawa and A. J. McEvily, Scripta Met., 15, 663 (1981).

26. T. H. Sanders, Jr. and E. A. Starke, Jr., Met. Trans., 7A, 1407 (1976).

27. H. Mughrabi and R. Wang, Proc. 2nd Risø Intl. Symp. on Met. and Mater. Sci., Roskilde, Denmark, to be published in the Proceedings (1981).

28. H. C. Heikkenen, M.S. Thesis, Georgia Institute of Technology (1981).

29. J. K. Lee and C. Laird, Mat. Sci. and Eng., in press.

30. T. H. Sanders, Jr. and E. A. Starke, Jr. eds., Aluminum Lithium Alloys, TMS-AIME (1981).

31. E. A. Starke, Jr., T. H. Sanders, Jr. and I. G. Palmer, J. of Metals 33, 24 (1981).

32. K. K. Sankaran and N. J. Grant, Aluminum-Lithium Alloys, T. H. Sanders, Jr. and E. A. Starke, Jr., eds., TMS-AIME, 205 (1981).

33. T. H. Sanders, Jr., Final Report, Naval Air Development Center, Contract No. N62269-76-C-0271, (1979).

34. A. Gysler, R. Crooks, and E. A. Starke, Jr., Proceedings of the 7th International Light Metals Congress, Leoben-Vienna, Austria (1981).

35. E. Hornbogen and K. H. Zum Gahr, Metallography 8, 181 (1975).

36. D. B. Williams, Aluminum-Lithium Alloys, T. H. Sanders, Jr. and E. A. Starke, Jr., eds., TMS-AIME, 89 (1981).

37. S. Ceresara, G. Cocco, G. Fagherazzi and L. Schiffini, Phil. Mag. 35, 373 (1977).

38. B. Noble and G. E. Thompson, Metal Sci. J. 5, 114 (1971).

39. M. Tomura, T. Mori and T. Nakamura, J. Japan Inst. Met. 34, 919 (1970).

40. D. B. Williams and J. W. Edington, Metal Science 9, 529 (1975).

41. T. H. Sanders, Jr., E. A. Ludwiczak and R. R. Sawtell, Mat. Sci. Engr. 43, 247 (1980).

42. J. C. Fisher, Acta Met. 2, 9 (1954).

43. J. B. Cohen, J. Mat. Sci. 4, 1012 (1969).

44. P. M. Kelly, Int. Met. Rev. 18, No. 17C, 31 (1973).

45. M. Meuris and E. Hornbogen, Practical Metallography 13, 160 (1976).

46. B. Chakravartti, E. A. Starke, Jr., and B. G. LeFevre, J. Mat. Sci. 5, 394, (1970).

71. J. M. Silcock, Phil. Mag., Vol. 4, 1187 (1959).

72. A. J. Perry, Acta Met., Vol. 14, 1143 (1966).

73. P. Bardhan and E. A. Starke, Jr., J. Mat. Sci., Vol. 3, 577 (1968).